Meteorol Atmos Phys 82, 5–29 (2003)
DOI 10.1007/s00703-001-0584-9

Meteorology and Atmospheric Physics
Printed in Austria

[1] Department of Atmospheric Science, Colorado State University, Fort Collins, CO
[2] Mission Research Corp./ASTeR Div., Fort Collins, CO
[3] Department of Meteorology, The Pennsylvania State University, University Park, PA

# RAMS 2001: Current status and future directions

**W. R. Cotton[1], R. A. Pielke Sr.[1], R. L. Walko[2], G. E. Liston[1], C. J. Tremback[2], H. Jiang[1], R. L. McAnelly[1], J. Y. Harrington[3], M. E. Nicholls[1], G. G. Carrio[1],** and **J. P. McFadden[1]**

With 7 Figures

Received March 12, 2001; revised August 28, 2001
Published online: November 21, 2002 

**Summary**

An overview of the Regional Atmospheric Modeling System (RAMS) is presented. We focus on new developments in the RAMS physics and computational algorithms since 1992. We also summarize some of the recent applications of RAMS that includes synoptic-scale weather systems and climate studies, to small-scale research using RAMS configured as a large eddy simulation model or to even flow around urban buildings. The applications include basic research on clouds, cloud systems, and storms, examination of interactions between tropical deep convective systems and ocean circulations, simulations of tropical cyclones, extreme precipitation estimation, regional climatic studies of the interactions between the atmosphere and the biosphere or snow-covered land-surfaces, prototype realtime mesoscale numerical weather prediction, air pollution applications, and airflow around buildings.

## 1. Introduction

RAMS, which was developed at Colorado State University and MRC/*ASTeR, is a multipurpose, numerical prediction model that simulates atmospheric circulations ranging in scale from an entire hemisphere down to large eddy simulations (LES) of the planetary boundary layer. It is most frequently used to simulate atmospheric phenomena on the mesoscale (horizontal scales from 2 km to 2000 km) for applications ranging from operational weather forecasting to air quality regulatory applications to support of basic research. RAMS has often been successfully used with much higher resolutions to simulate boundary layer eddies (10–100 m grid spacing), individual building simulation (1 m grid spacing), and direct wind tunnel simulation (1 cm grid spacing). RAMS' predecessor codes were developed to perform research in modeling physiographically driven weather systems and simulating convective clouds, mesoscale convective systems, cirrus clouds, and precipitating weather systems in general. RAMS use has increased to more than 120 current RAMS installations in more than 30 different countries.

The RAMS concept was created in the early 1980's at Colorado State University by merging three related models: the CSU cloud/mesoscale mode (Tripoli and Cotton, 1982), a hydrostatic version of the cloud model (Tremback, 1990), and the sea breeze model described by Mahrer and Pielke (1977).

The original RAMS was run exclusively on the NCAR CRAY-1 machine. That machine's small central memory (1 Mword or 8 Mbytes) forced various design constructs that limited its

application to what we would consider today to be small runs. When computers with significantly more memory became available the entire RAMS code was rewritten, obsolete features were removed, and parameterizations from the sea breeze model were included. The first version of the ''new'' RAMS was released in 1988 as version 0a, and the first widely distributed version, version 2c, was released in 1991.

A key issue in RAMS development was taking full advantage of modern parallel computer capabilities. RAMS first parallel version was developed at CSU in 1991. Message Passing Interface (MPI) did not exist then, so Parallel Virtual Machine (PVM) was used for the message-passing package. An essentially complete version was finished in 1994, support for MPI was implemented in 1995, and a prototype operational version of the parallel RAMS was installed at Kennedy Space Center in late 1995. RAMS is well suited for parallelization since it does not use global physical/numerical routines. For example, it calculates pressure locally and non-hydrostatically using a time-split compressible approximation. Also, advection is calculated using local finite difference operators rather than non-local spectral methods.

## 2. Summary of RAMS options

The current released version of RAMS is designated as version 4.3. RAMS provides a broad range of options that allow it to be tailored for a wide range of applications. The code contains a variety of structures and features ranging from non-hydrostatic codes, resolution ranging from less than a meter to a hundred kilometers, domains from a few kilometers to the entire globe, and a suite of physical options. This allows users to easily select appropriate options for different spatial scales, meteorological problems or applications, or locations.

RAMS has a multiple grid nesting scheme that lets it solve the model equations simultaneously on any number of interacting computational meshes of differing spatial resolution. The highest resolution meshes are used to model details of small-scale atmospheric systems, such as flow over complex terrain and surface-induced thermal circulations. Coarse meshes are used to model the environment of these smaller systems

**Table 1.** Range of options for configuring RAMS

| | |
|---|---|
| Basic equations | – Non-hydrostatic time-split compressible |
| Dimensionality | – 2-dimensional<br>– 3-dimensional |
| Vertical coordinate | – Standard Cartesian coordinate<br>– Terrain-following height coordinate<br>– Terrain Intersecting Cartesian coordinate (shaved ''ETA''-type)** |
| Horizontal coordinate | – Rotated polar-stereographic transformation<br>– Global domain option |
| Grid structure | – Arakawa-C grid stagger<br>– Unlimited number of nested grids<br>– User-specified space and time-step nesting ratios<br>– Ability to add and subtract nests<br>– Moveable nests |
| Time differencing | – Hybrid combination of leap-frog and forward-in-time |
| Turbulence closure | – Smagorinsky (1963) deformation-K closure scheme with stability modifications made by Lilly (1962) and Hill (1974)<br>– Deardorff level 2.5 scheme – eddy viscosity as a function of TKE<br>– Mellor-Yamada level 2.5 scheme – ensemble–averaged TKE (Mellor and Yamada, 1982)<br>– Kosovic (1997) sub-grid scheme* |
| Cloud microphysics | – Warm rain processes<br>– Five ice condensate species<br>– Level 1 – No cloud<br>– Level 2 – Condensation only<br>– Level 3 – Single-moment bulk scheme – Walko et al (1995)<br>– Level 4 – Two-moment bulk scheme – Meyers et al (1997). Levels 3 and 4 both with look-up table bin-micro for autoconversion and sedimentation (Feingold et al, 1998) and non-hydrometeor thermo (Walko et al, 2000)<br>– Level 5 – full bin-resolving two-moment scheme – University of Tel-Aviv, Tzivion et al (1987) and Reisin et al (1996)* |

(*continued*)

**Table 1** (*continued*)

| | |
|---|---|
| Convective | – Modified Kuo – Tremback (1990) |
| Parameterization | – Rafkin (1996)*<br>– Pan-Randall (1998)*<br>– Frank-Cohen (1987)*<br>– Weissbluth (1991)* |
| Radiation | – Mahrer and Pielke (1977) long/shortwave model – no cloud processes<br>– Chen and Cotton (1983) long/shortwave model – cloud processes considering all condensate as liquid<br>– Harrington (1997) long/shortwave model – two-stream scheme interacts with liquid and ice hydrometeor size-spectra |
| Lower boundary | – Soil/vegetation/snow parameterization – LEAF-2 (Walko et al, 2000)<br>– Ocean surface-coupled ocean model – Costa et al (2001a, b)*<br>– Snow surface coupled model – Liston et al (1999)* |
| Upper boundary condition | – Rigid lid<br>– Rigid lid with a high-viscosity layer aloft to damp gravity waves, by nudging to large-scale analysis or initial conditions |
| Lateral boundary condition | – Klemp and Wilhelmson (1978) radiative condition<br>– Large-scale nudging boundary conditions – Davies (1983)<br>– Cyclic or periodic boundaries |
| Initialization | – Horizontally homogeneous from a single sounding<br>– RAMS/ISAN package – hybrid isentropic/terrain following analysis using gridded larger scale model data combined with large variety of observed data types – Tremback (1990) |
| Data assimilation | – Four-dimensional "analysis" nudging to data analyses |
| Computer aspects | – Operating systems: UNIX, LINUX, MS Windows 95/98/NT/2000<br>– Parallel processing on distributed and shared memory platforms using Message Passing Interface (MPI) |

* Option only in research versions at Colorado State University

** Option under development

and provide boundary conditions for the fine mesh regions. Coarse meshes are also used to simulate large scale atmospheric systems that interact with the smaller-scale systems resolved on the finer grids.

Table 1 summarizes the principal options available in RAMS.

## 3. Major new developments in RAMS physics and computational algorithms

We will now describe some of the major new developments in RAMS physics and computational algorithms since our 1992 summary (Pielke et al, 1992a). RAMS updates are also reported in Pielke (2001b), and Nicholls et al (1995).

### *3.1 Microphysics*

The work of Verlinde et al (1990), which showed that analytical solutions to the collection equation were possible when applied to predictions of hydrometeor mixing ratio and concentrations, spearheaded a major change in the philosophical approach to cloud parameterization in RAMS. Instead of using continuous accretion approximations as had been the norm in cloud parameterizations, they showed that solutions to the full stochastic collection equation can be obtained subject to approximations (i.e., the collection efficiencies are constant). This approximation is typically used as well in classical bulk parameterization schemes that follow Kessler's (1969) basic approach. Walko et al (1995) describe the implementation of this approach in RAMS for prediction of hydrometeor mixing ratios. An important aspect of the implementation strategy was the use of look-up tables that enabled fast and accurate solutions to the collection equations. The lookup tables contain solutions to the stochastic collection equation as a function of (1) the pair $(x, y)$ of interacting species, (2) the characteristic diameter of species x, and (3) the characteristic diameter of species y. Other factors such as air density, number concentrations of x and y, and collection efficiency appear outside the double integral of the stochastic collection equation and therefore are not part of the table. Meyers et al (1997) then extended this approach to two-moments of the hydrometeor spectra:

mixing ratio and number concentration. Also in Verlinde et al and subsequent implementations in RAMS, the Kessler-type exponential or Marshall-Palmer basis function for hydrometeor spectra was abandoned in favor of a generalized gamma distribution function,

$$n(D) = \frac{N_t}{\Gamma(\nu)} \left( \frac{D}{D_n} \right)^{\nu-1} \frac{1}{D_n} \exp\left( - \frac{D}{D_n} \right), \qquad (1)$$

where $n(D)$ is the number of particles of diameter $D$, $N_t$ is the total number of particles, $v$ is the shape parameter, and $D_n$ is some characteristic diameter of the distribution. The Marshall-Palmer (exponential) and Khrgian-Mazin distribution functions are special cases of this generalized function. When two-moments of a hydrometeor class is predicted, all that is needed to completely specify the distribution function given by (1) is the specification of $\nu$. Except for the few cases where observations can be used to specify $\nu$, its value is chosen by trial and error or altered in sensitivity experiments.

Owing to the use of look-up tables, it became apparent that it is no longer necessary to constrain the system to constant or average collection efficiencies. Thus Feingold et al (1998) replaced the formerly ad hoc autoconversion formulations in RAMS with full stochastic collection solutions for self-collection among cloud droplets and for rain (drizzle) drop collection of cloud droplets. The look-up tables were then computed using realistic collection kernels rather than constant collection efficiencies used in the past. The philosophy of bin representation of collection was also extended to calculations of drop sedimentation. Previously, bulk microphysics schemes have treated sedimentation of hydrometeors by integrating over the entire particle size-spectra and obtaining a mass-weighted fall speed. The closest agreement between a full bin-resolving microphysics model in a large eddy simulation (LES) of marine stratocumulus cloud and the bulk microphysics representation was obtained when both collection and sedimentation were simulated by emulating a full-bin model having 36 bins. Bin sedimentation is simulated by dividing the gamma distribution into discrete bins and then building look-up tables to calculate how much mass and number in a given grid cell fall into each cell beneath a given level in a given time step.

Among other refinements in the bulk microphysics model, was the introduction of a mass and energy-conserving heat-budget equation for the larger precipitating hydrometeors so that heat storage on these species is permitted. In addition, hydrometeors such as hailstones can be represented as mixed-phase hydrometeors when they are diagnosed to be undergoing wet growth (see Walko et al, 1995; 2000). Furthermore, Walko et al (2000) describe an implicit algorithm for representing diffusion of sensible heat and vapor between hydrometeors and air that is stable for long time steps yet does not require iteration.

Cloud droplet number may be predicted from a specified constant cloud condensation nuclei (CCN) concentration or from a fully prognosed CCN field. The number of CCN that activate are a function of air temperature, Lagrangian supersaturation production rate (related to vertical velocity and other factors) and number concentration of CCN. Other factors such as CCN chemistry, mean radius, and spectral width are considered fixed for a given RAMS simulation. Based on the above CCN characteristics and environmental factors, the fraction of CCN that nucleate into cloud droplets is accessed in RAMS from a lookup table that was previously generated from a detailed bin-parcel model. Prediction of CCN in RAMS includes advective and diffusive transport, source functions, and nucleation scavenging.

For ice-phase clouds, the ice nucleation models have been changed dramatically. In Cotton et al (1986) ice nucleation by deposition/condensation-freezing was parameterized using Fletcher's (1962) formula while contact nucleation was modeled following Young (1974a, b). The Fletcher formula tends to under-estimate ice crystal concentrations at warm temperatures and over-estimates them at cold temperatures. Moreover, the Young contact nucleation model dominated over the Fletcher formula in ice production. In Meyers et al (1992), the Fletcher formula was replaced with a new formula derived from published continuous flow diffusion chamber data sets. The formula used is

$$N_{id} = \exp\{a + b[100(S_i - 1)]\},$$

where $N_{id}(l^{-1})$ is the number of pristine ice crystals predicted due to deposition–condensation freezing, $a = -0.639$, $b = 0.1296$, and $S_i$ is ice

saturation ratio. In addition, Young's estimates of contact nuclei concentration were replaced with estimates from laboratory experiments by Vali (1974; 1976), Cooper (1980), and Deshler (1982). The formula for contact nucleation takes the form:

$$N_{\rm ic} = \exp[a + b(273.15 - T_c)],$$

where $a = -2.80$ and $b = 0.262$, is used [units of $N_{\rm ic}$ are inverse liters ($l^{-1}$)]. This altered the primary ice nucleation processes such that contact nucleation became secondary to ice production by deposition/condensation–freezing. In version 4.3 we have added an option to predict the vertical and horizontal transport of ice-forming nuclei (IFN). Thus in cases where soundings of IFN are available we now have the capability of predicting the vertical mixing and transport of IFN from high to low concentration regions and vice versa.

The secondary ice particle production model in RAMS is based on Mossop (1978) in which he derived the empirical relation:

$$\mathrm{N}_i = \mathrm{c}\,\mathrm{N}_{24}(\mathrm{N}_{13})^{\mathrm{m}}, \qquad (2)$$

where $\mathrm{N}_i$ is the number of ice particles produced per second, $\mathrm{N}_{24}$ is the number of cloud droplets larger than 24 microns in diameter that are collected by ice each second, $\mathrm{N}_{13}$ is the number of cloud droplets smaller than 13 microns in diameter that are collected by ice each second, m is an exponent equal to 0.93, and c is a constant of proportionality. This relationship was derived from a laboratory apparatus in which supercooled cloud droplets were collected on a glass rod, and experiments were conducted for a wide range of droplet concentrations, leading to many different values of $\mathrm{N}_{24}$ and $\mathrm{N}_{13}$.

We re-interpreted the empirical results of Mossop by accounting for the cross-sectional area of the glass rod, which was 5.4 $\mathrm{cm}^2$. In RAMS, we thus compute $\mathrm{N}_{24}$ and $\mathrm{N}_{13}$ per 5.4 $\mathrm{cm}^2$ of cross sectional area of ice particles that collect cloud water, and apply the above formula.

In MKS units, the formula is:

$$\mathrm{N}_i = 9.\exp(-10) \times B \times \mathrm{N}_{24} \times (\mathrm{N}_{13})^{0.93}, \qquad (3)$$

where $B$ increases linearly from 0 to 1 as ice temperature $T$ increases from $-8\,\mathrm{C}$ to $-5\,\mathrm{C}$, $B$ decreases linearly from 1 to 0 as $T$ increases from $-5\,\mathrm{C}$ to $-3\,\mathrm{C}$, and $B$ is zero at other ice temperatures.

At colder temperatures such as found in cirrus clouds, primary nucleation by homogeneous freezing of supercooled cloud drops and haze particles was introduced (DeMott et al, 1994).

With these changes in primary and secondary nucleation models in RAMS, we find that the model more consistently predicts ice crystal concentrations within a factor of ten of observed amounts. Still, we believe the model would have difficulty in predicting the very rapid ''stage-2'' formation of ice crystals in cumulus clouds observed by Hobbs and Rangno (1985), and Rangno and Hobbs (1991; 1994).

Other changes in the ice microphysics from Cotton et al (1986) involve a re-definition of ice particle categories. Formerly, ice particles were categorized as pristine crystals, aggregates, and graupel particles. Now ice is categorized into pristine ice, which is pure vapor-grown crystals, and snow, which is larger vapor-grown crystals and crystals that undergo moderate riming (Harrington et al, 1995). Aggregates remain as a separate category, as well as low-density graupel particles. Hail is an additional category that represents high-density frozen particles such as frozen raindrops and hailstones.

In addition to the bulk microphysics schemes in RAMS, it also contains options for using the bin-resolving multi-moment schemes developed at the University of Tel-Aviv (Tzivion et al, 1987; Reisin et al, 1996). These computationally expensive options are used in rather simple cloud systems such as boundary layer clouds and in the refinement of the bulk microphysics model such as in Feingold et al (1998).

### *3.2 The cloud radiation scheme*

A new two-stream radiation scheme developed by Harrington (1997; see also Harrington et al, 1999) is now available in RAMS, which treats the interaction of three solar and five infrared bands with the model gases and cloud hydrometeors. The older Chen and Cotton (1987) scheme used a two-stream model for solar radiation and an emissivity approach to longwave radiation. The emissivity approach has the disadvantage that the computational costs go up with the square of the number of levels whereas a two-stream model costs go up linearly with the number of vertical levels. For high-vertical resolution

simulations this scheme became very costly compared to the new two-stream scheme in the infrared. Moreover, the Chen–Cotton scheme only interacted with the bulk liquid or ice condensate simulated by RAMS. The new model, responds to the detailed liquid and ice hydrometeor size-spectra simulated with both the bulk and bin-resolving microphysics models (Harrington and Olsson, 2001a). This permits simulation of changes in radiative heating as droplet spectra broaden to precipitation sizes and even feedbacks of radiation on droplet and ice particle vapor deposition growth (Harrington et al, 1999; Wu et al, 2000).

### *3.3 Land-surface model*

The RAMS land surface model has increased in sophistication over the last several years with the addition of vegetation, canopy air, snowcover, and surface hydrology to the underlying soil model. Earlier versions of the RAMS land surface model are reported in McCumber (1980), McCumber and Pielke (1981), Tremback and Kessler (1985), and Lee et al (1995). The current version, known as LEAF-2 (Walko et al, 2000) represents the storage and exchange of heat and moisture associated with the atmosphere–terrestrial interface. The latent heat fluxes are evaluated separately for evaporation from the soil and from intercepted water on vegetation, and for transpiration through the stomata on plants. The water budget is similarly treated and includes a subgrid representation of run-off using a version of TOPMODEL (Band, 1993). Vegetation may be multilayered in terms of leaf area index, but is represented by a single prognostic temperature and surface moisture (dew or intercepted rainfall). Surface physiography can be assigned to an individual grid column based on either a single predominant type, which is suitable for cloud-resolving grid spacing, or as a mosaic of different types, which becomes more important with more varied physiography over larger grid cells. Lu (1999) has interfaced LEAF-2 to the CENTURY ecology model, which permits simulations on time-scales of seasons or years by simulating growth and decay of plant species in the biosphere, in response to changes in seasons, radiation, and precipitation. Typically 10 or 12 soil levels are used in LEAF-2, but any number of levels can be selected.

RAMS has been used in a variety of studies to demonstrate the role of landscale variability and change over time in the generation of mesoscale wind flow. These studies include Pielke et al (1991a; 1993; 1999a, b), and Stohlgren et al (1998). A review of the role of land surface models in atmospheric models, including application of LEAF-2 in RAMS is given in Chen et al (2001). Taylor et al (1998) has shown using RAMS that variations of snow cover in the boreal forest can generate mesoscale flow. Pielke and Uliasz (1993) illustrated how atmospheric dispersion is influenced by landscape variability.

### *3.4 Snow evolution model*

The problem of realistically representing seasonal snow in regional atmospheric and hydrologic models is made complex because of the numerous snow-related features that display considerable spatial variability at scales below those resolved by the models. As an example of this variability, over the winter landscape in middle latitudes the interactions between wind, vegetation, topography, precipitation, solar radiation, and snowfall produce snow covers of nonuniform depth and density (e.g., Elder et al, 1991; Sturm et al, 1995; Liston and Sturm, 1998). During the melt of such snow covers, the snow-depth variation leads to a patchy mosaic of vegetation and snow cover that evolves as the snow melts (e.g., Shook et al, 1993; Liston, 1999). Because of the large differences in the albedo of land/vegetation, sea ice, and snow, knowledge of the fractional snow-covered area is crucial in determining the surface energy flux interactions between the land, snow, sea ice, and atmosphere (Liston, 1995).

As part of our snow-modeling efforts we have developed a Subgrid SNOW Distribution (SSNOWD) model for use in regional and global atmospheric models, and large-scale hydrologic models (Liston, 2001). This work showed that accounting for subgrid snow distributions was required to successfully simulate snow–land–atmosphere processes and feedbacks. Our work has also shown that the subgrid snow distribution is the first-order influence on snow cover depletion during snowmelt (Liston, 1999). As part of the snow-model formulation, the fractional snow-covered area in each atmospheric model grid

cell, at each model time step, is defined. The snow-covered fraction is then used to partition the surface energy fluxes over the snow-covered and snow-free portions of each grid cell (Liston, 1995). The SSNOWD model has been implemented and tested in RAMS (Liston et al, 1999; Liston, 2001; Liston and Pielke, 2001).

Three inputs are required to run the subgrid snow-distribution model: (1) the total grid-cell accumulated snow precipitation (since the last time the grid cell was snow-free); (2) the total accumulated snowmelt (since the last time the grid cell was snow-free); and (3) a function and parameter(s) that describes the shape of the snow-distribution curve. In its simplest form, depending on the function used, the only parameter needed is the coefficient of variation describing the subgrid snow distribution. The inclusion of the first two, within the context of an atmospheric model, just requires the addition of two, two-dimensional accounting arrays in the model.

The third model input requires knowledge of how snow distributions vary from one region to another. Liston (2001) identified the processes that influence snow distributions and how they vary across the globe, and globally mapped eight different snow-distribution categories used by SSNOWD. These categories are the result of three main influences related to processes governing snow-distribution variability across various landscapes: (1) temperature, (2) topographic variability, and (3) wind speed. These factors influence such things as: solid precipitation amounts, solid orographic precipitation, snow-redistribution by wind, and solar radiation variations; all of which exert a strong influence on snow-depth spatial distribution and variability.

### *3.5 The ocean model*

Costa et al (2001a) have coupled a two-dimensional version of the Princeton Ocean Model (POM), described by Blumberg and Mellor (1987) to a two-dimensional cloud-resolving model (CRM) version of RAMS over the tropical western Pacific. The ocean model contains prognostic equations for the zonal and meridional currents, potential temperature, salinity, turbulent kinetic energy and turbulent length scale. A splitting procedure is adopted to resolve the fast-varying external mode and the slow-varying internal mode. The turbulence closure sub-model is the level 2.5 scheme in the hierarchy described by Mellor and Yamada (1974). Long-wave radiative fluxes are evaluated at the boundary. Shortwave radiation is allowed to penetrate the ocean and is treated as a source term of heat in each level. The present shortwave radiation scheme in the ocean is quite simple: no spectral dependence is considered and a single exponential attenuation is calculated for the whole radiative flux. No large-scale forcing was imposed on the ocean model.

The coupling formulation is similar to the one described by Hodur (1997). The models interchange momentum, heat and water substance. Information regarding the downward short and long-wave radiation at the ocean surface and the SSTs allows the calculation of the radiative fluxes. The ocean currents are neglected in the calculation of the surface heat and momentum fluxes.

In Sect. 4.3, we summarize some of the results of using this coupled version of RAMS.

### *3.6 The sea-ice model*

Sea-ice distributions and concentrations in RAMS are now prescribed using the National Oceanic and Atmospheric Administration (NOAA) automated passive microwave sea-ice concentration analyses generated at the National Centers for Environmental Prediction (NCEP). In these analyses the Special Sensor Microwave Imager (SSM/I) instrument, part of the Defense Meteorological Satellite Program (DMSP), is used to develop the sea-ice data sets (Cavalieri, 1992). These data sets are available daily, on a 0.5 by 0.5 degree global grid.

In this implementation, each model grid cell can now have a sea-ice fraction, along with a fractional snow cover over the land fraction, and an ice-free water fraction. By prescribing the sea-ice distributions and concentrations we focus on achieving an appropriate simulation of the surface energy fluxes when sea-ice is present. The model performs a complete surface energy balance over the sea-ice fraction, including the constraint that a melting surface cannot rise above 0 degrees C, and that energy may be available for snow and/or ice melt. The presence of sea-ice also modifies the surface properties like albedo and roughness.

Recently the Los Alamos National Laboratory predictive sea-ice model (Hunke and Lipscomb, 1999) has been implemented into RAMS. The thermodynamic module is much like the model of Maykut and Undesteiner (1971), with heat capacity, thermal conductivity and enthalpy of the sea-ice depending on both temperature and salinity. Different thicknesses (categories) of ice are allowed to be present within a grid cell area as large variations of ice thickness and growth rate typically occur. For each thickness category, the temperatures of the surface, the snow cover, and those corresponding to a specified number of internal ice layers are considered prognostic variables although, the corresponding salinity and density profiles are prescribed. The temperature at the midpoint of each internal ice layer is computed based on thermal conduction, and net energy fluxes at the top and bottom surfaces are used to calculate thickness changes in the snow and ice layers. Energy and mass are conserved whenever ice is transported in the thickness space using the linear remapping scheme of Lipscomb (2000).

Routines have been included to evaluate the surface momentum fluxes corresponding to each thickness category (and open sea), and various minor improvements have been made to those modules in the original sea-ice package involved in the coupling with RAMS such as the sensible and latent heat fluxes. In the original code, a single exponential attenuation is used to take into account the fraction of the incoming solar radiation that penetrates the snow and ice layer, therefore the treatment of the downward short wave radiation (and albedo) has been modified to include a spectral dependence. The radiation scheme previously implemented in RAMS (Harrington, 1997) was also modified to take the cloud fraction into account, in order to provide an adequate radiative coupling of the surface information generated by the sea-ice modules and the atmospheric model.

Observed divergence and shear rates such as those obtained during the SHEBA (Surface HEat Budget of the Arctic Ocean) project are used to take into account the ridging process. However, for simulations with a coupled ocean model, a different treatment for sea-ice dynamics is being explored as a compromise solution between the rather complex Flato and Hibler's (1995) and highly parameterized description of column models.

The coupled model can be used for one, two, and three-dimensional simulations, and the original initialization routines have been modified to include a wide variety of options for initialization according to the available ice thickness data. This version of RAMS coupled with the sea-ice model avoids the need to directly specify the large-scale vertical motion and the time-varying advective tendencies of temperature and moisture in simulations focused in the sea-ice evolution. It also provides more realistic turbulent surface fluxes and albedo to the atmospheric model for cloud simulations over Arctic interior ice regions. This last aspect will be of great relevance for the studies on Arctic Basin clouds and their implications on climate.

### *3.7 Global extension of RAMS*

The choice of polar stereographic horizontal coordinates in RAMS is ideal for limited area modeling anywhere on the earth because it avoids the singularities at the geographic poles that are inherent in a latitude–longitude system. However, polar stereographic coordinates cannot be extended over the entire sphere. By coupling two hemispheric polar stereographic grids for full coverage of the earth's surface, RAMS has been extended to a global modeling capability. As for the limited area application of RAMS, a hemispheric grid may be positioned at any location on the earth (with the other hemispheric grid exactly opposite), and grid nesting within either or both hemispheric grids may be used. This allows a variety of useful studies of high-resolution interaction at local and regional scales with large-scale features such as El Niño.

## 4. Some examples of applications of RAMS

### *4.1 RAMS in LES mode*

RAMS has been applied to the large eddy simulation of marine stratocumulus clouds, Arctic stratus clouds, and cumulus clouds in the last few years. Using large eddy simulations that incorporate bin-resolving microphysics, Stevens et al (1998) examined the influence of drizzle formation on the structure and dynamics of

marine stratocumulus clouds. They showed that for cases in which the overlying air is close to sea surface temperatures, evaporation of drizzle below cloud base promotes a cooler and moister subcloud layer that inhibits deep mixing. The stabilized sub-cloud layer subsequently builds up convective available potential energy (CAPE) at low levels resulting in the formation of cumuli rising out of the sub-cloud layer and penetrating into the stratus deck. The cumuli-under stratus are responsible for most of the heat and moisture transport and generate circulations in the boundary layer which differs markedly from the non-drizzling boundary layer.

According to existing data, giant sea-salt CCN with radii greater than about 1 micron exist in the marine boundary layer at concentrations of about $10^{-4}$ to $10^{-3}\,\mathrm{cm}^{-3}$, depending on the size of the particles and the sea-state. Feingold et al (1999) evaluated the extent to which observed concentrations of giant CCN affect drizzle formation. The models show a consistent picture with perceptible drizzle being initiated up to an hour earlier when giant CCN exist. The study also shows that the albedo susceptibility of clouds depends upon the availability of giant CCN.

It has been suggested that longwave cooling has the potential to enhance the formation of drizzle-sized drops by allowing the latent heat generated during condensation to be dissipated more rapidly than through standard diffusion theory. By coupling a multi-band two-stream model to the droplet growth equations, (Harrington et al, 2000) quantified this impact within a trajectory ensemble model, and in a two-dimensional CRM of summertime Arctic stratus. Results indicate that droplets that experience significant cloud top residence times – the region of the cloud where radiative cooling is most tangible – produce drizzle far more rapidly when radiation is coupled to droplet growth.

Simulations of drizzling tradewind cumulus clouds for an idealized BOMEX case study by Jiang and Cotton (2000) revealed that drizzle leads to reduced buoyancy fluxes and less turbulence. Consequently drizzling boundary layers appear to entrain less than their non-drizzling counterparts. This is consistent with the simulation of a drizzling marine stratocumulus boundary layer by Stevens et al (1998). Heavy drizzle events are simulated in association with deeper clouds, which get as high as 2 km when prescribed large-scale cooling was replaced by a two-stream radiative parameterization. When microphysics and drizzle are excluded in the simulation, the impact of the radiative parameterization on the cloud fields is minor.

In an idealized, two-dimensional CRM simulation, Harrington et al (1999) showed that the simulated Arctic stratus is very sensitivity to the concentration of IFN. Jiang et al (2000; 2001) extended those simulations using a cloud-resolving model to examine one of the cases of Arctic mixed-phase boundary layer clouds observed during the Beaufort and Arctic Seas Experiment. We found that the simulated stratus cloud is very sensitive to the concentration of ice crystals. Using middle-latitude estimates of the availability of ice nuclei, we find that the concentrations of ice crystals is large enough to result in the almost complete dissipation of otherwise solid, optically-thick stratus layers. A tenuous stratus can be maintained when the continuous input of moisture through large-scale advection is strong enough to balance the ice production. By reducing the concentration of IFN to 0.3 of the mid-latitude estimated values, a persistent, optically thick stratus layer was maintained. The longwave radiative fluxes at the surface differred by $50\,\mathrm{watts/m}^2$ between solid stratus and the glaciated stratus simulations. This suggests that transition-season Arctic stratus may be very vulnerable to anthropogenic sources of IFN, which can alter cloud structure sufficiently to affect the rates of melting and freezing of the Arctic Ocean.

During the Surface HEat Budget of the Arctic Ocean First International Satellite Cloud Climatology Project Regional Experiment (SHEBA/FIRE) spring intensive observational period (IOP) (May 18, 1998) a high concentration of CCN in the air above the cloud was observed to over-lie a fairly clean boundary layer. To understand how the microphysical and dynamical structure and radiation properties of Arctic stratus are modified by the entrainment of ''polluted'' air at cloud top in the arctic environment, Jiang et al (2001) performed two large eddy simulations of the FIRE/SHEBA May 18 case with liquid-phase, bin-resolving microphysics (Feingold et al, 1996). One simulation has the

initial CCN concentration set to $30\,cm^{-3}$ (low CCN) and the other uses the observed CCN data (high CCN). The simulation with the observed CCN profile (high CCN) showed that the increase in CCN concentration resulting from entrainment results in higher droplet concentrations, smaller drop sizes, more liquid water retained in the cloud layer, and less drizzle reaching the surface. The smaller drops also cause a decrease in the surface shortwave flux. The differences between the high CCN run and the low CCN run show characteristics of the differences between drizzling and non-drizzling clouds (e.g., Stevens et al, 1998), namely that drizzle redistributes heat and vapor in the vertical in a manner that stabilizes the boundary layer.

The LES mode of RAMS has been used to simulate the development of thermal internal boundary layers and roll cloud circulations that frequently occur in the Arctic during periods when cold air flows off of the arctic pack ice and over the warm open ocean. Olsson and Harrington (2000) used a nested 2-D version of LES in a large-domain simulation of cloudy boundary layer evolution during off-ice flow. Even though the surface forcing was very strong (around $700\,W\,m^{-2}$), the results of these model studies showed that the evolution of the boundary layer was heavily impacted by the inclusion of ice-phase microphysics. Boundary layer turbulence was much weaker with concomitant reductions in both cloud and boundary layer depth. Furthermore, Olsson and Harrington (2000) showed that the inclusion of detailed microphysics had a large impact on the strength of the mesoscale divergence near the ice edge. This was a very interesting example of microscale processes affecting the larger scale flow. Because of the strong influence of ice microphysics, a follow-up study by Harrington and Olsson (2001b) illustrated that the results showed a further sensitivity to ice nucleation and IFN.

In a set of 3-D LES simulations of the same case, Harrington and Olsson (2001c) showed that boundary layer roll development and clouds streets were dependent on the inclusion of ice microphysics. Simulations that included only liquid-phase microphysics produced very strong rolls that are relatively closely spaced and a domain that is completely cloud covered. In contrast, simulations that include ice microphysics have roll updraft regions that are cloudy, while the downdraft regions are completely cloud free. Furthermore, the boundary layer turbulence is weaker, boundary layer depth is shallower, and the rolls have wider spacing (closer to observations) than the case where pure liquid clouds were simulated.

The LES version of RAMS has also been applied to investigate the role of land surface heterogeneity on boundary layer dynamics. Eastman et al (1998) demonstrated the crucial role of spatial variation of soil moisture on lower atmospheric processes over the First ISLSCP (International Satellite Land Surface Climatology Project) Field Experiment (FIFE) area of Kansas. Vidale et al (1997) used LES RAMS to demonstrate that even with strong winds, the heterogeneity of the boreal forest landscape produces significant spatially varying turbulent and mesoscale fluxes. Pielke et al (1998) showed that when cumulus cloud development occurs, the influence of small-scale landscape heterogeneities is amplified relative to clear sky conditions. Walko et al (1992) and Hadfield et al (1991; 1992) explored the importance of small-scale terrain variations on the development of the convective boundary layer using LES versions of RAMS.

### *4.2 Cirrus simulations*

Simulating cirrus clouds is complicated for several reasons. First of all, being high in the troposphere, they are dominated by ice-phase microphysics. Nucleation of ice crystals can be both by heterogeneous nucleation and homogeneous freezing of supercooled droplets and haze particles. The concentrations of ice crystals then is controlled by supersaturations generated by cooling rates in the atmosphere created by large-scale lifting, gravity waves, and radiative cooling, as well as the concentrations of IFN, CCN (that determine concentrations of cloud droplets) and haze particles. In the tropics, in particular, deep convective clouds can trigger gravity waves, and transport large quantities of water substance, as well as CCN/haze/IFN particles, into the upper troposphere. Moreover, optically-thick cirrus clouds experience cloud-top radiative cooling which can destabilize the cloud layer and generate convective overturning

much like boundary layer stratocumulus clouds. Thus modeling cirrus clouds is a mesoscale problem, a deep convection problem, a small-scale turbulence problem, and involves complicated ice-phase nucleation and crystal growth processes.

RAMS was first applied to simulating cirrus clouds by Heckman and Cotton (1993) as a mesoscale model with grid spacing of 100 km and 33 km. The case was the FIRE 28 October 1986 (Starr, 1987), over the central U.S. The simulation depicted many of the observed dynamic and cloud fields including cloud height, thickness, areal extent, and cloud microphysical composition. Moreover, the model produced weak convective-like activity that enhanced the cloud optical depth.

In an exploratory study of tropical cirrus, Mitrescu (1998) performed two- and three-dimensional cloud-resolving simulations of tropical cirrus. The case was the 22 December 1992 Tropical Ocean Global Atmosphere–Coupled Ocean–Atmosphere Research Experiment (TOGA–COARE) case used for model intercomparison studies as a part of GEWEX Cloud Systems Study Program (GCSS) Working Group #4. These simulations were initialized and then nudged using two-dimensional CRM output data obtained from the RAMS participation in that study. The vertical grid spacing was stretched from 150 m to 1.0 km up to almost cirrus levels in the lower troposphere, then contracted to 50 m spacing in the cirrus layer. A horizontal grid spacing of 100 m was used over the 50 km domain. The three-dimensional simulation produced a stable thick cirrus cloud with a base at 8000 m and top at 11,200 m, and below that layer, a cloud layer consisting of mostly aggregates was separated from the layer above by a dry layer.

Wu (1999) used a combination of mesoscale simulations, three-dimensional LES with bulk microphysics, and two-dimensional CRM with bin-resolving microphysics to study the physics and dynamics of the 26 November 1991 FIRE II cirrus case described by Mace et al (1995). The mesoscale simulation was set up with horizontal grid spacing of 80 km, 20 km, and 4 km, respectively. The finest grid was placed over a thin cirrus cloud (Case 1), and a fourth grid of 1 km spacing was added, and then placed over a deep layer cloud (Case 2), but with only three grids. Similar to Mitrescu's simulations, the vertical grid structure varied from modestly coarse in the lower troposphere and then refined to 200 m at cirrus levels. RAMS was initialized with the Mesoscale Analysis and Prediction System (MAPS; Benjamin et al, 1991) analyses enhanced with soundings. The mesoscale simulation produced three cloud bands similar to observations, with cloud optical depths similar to observations, although the positions of the cloud bands were more to the northwest.

Soundings in the vicinity of the model-predicted thin cirrus cloud (Case 1) and the deeper cirrus/stratus (Case 2) were extracted from the mesoscale simulation and used to initialize an LES model set up with 150 m horizontal grid spacing and 50 m vertical spacing in the cloud layers. The LES model was nudged with large-scale forcing derived from the mesoscale simulation. As described by Wu (1999), and Cheng et al (2001), the LES model developed a thin cloud layer in which latent heat release was small relative to radiative heating, and a thick cloud layer with embedded convective cells where latent heating was important to the cloud dynamics and structure. These two cloud regimes were very different in character. In both the mesoscale and LES simulations the RAMS two-moment bulk microphysics was used.

For the thin cirrus case, Wu et al (2000) examined the importance of radiative heating and cooling to the dynamics and microphysics of the thin and thick cirrus layers. In this case RAMS was interfaced to Reisin et al (1996) bin-resolving microphysics model with a radiation term added to the vapor diffusion equation and the supersaturation equation. Using the soundings extracted from the mesoscale simulation in the vicinity of the thin and thick cloud layers, a two-dimensional analog of the LES model was set up. The simulations revealed that solar plus terrestrial radiative heating had a significant impact on the evolution of the size-spectra of the ice hydrometeors, producing a reduction of hydrometeor mass and even altered the dynamics of the simulated cloud layer. Owing to the larger radiative cross section of larger ice particles, large ice particles experience so much radiative warming that saturation vapor pressures become large enough to cause their

sublimation, while smaller crystals with small radiative cross sections continue to grow by vapor deposition.

### *4.3 Coupled atmosphere ocean simulations*

In order to study the interactions between deep convection and the upper ocean over the tropical western Pacific, Costa et al (2001a) interfaced the two-dimensional cloud-resolving version of RAMS to the Princeton Ocean Model (POM) described by Blumberg and Mellor (1987). The coupling formulation is similar to the one described by Hodur (1997). The models interchange momentum, heat and water substance. Information regarding the downward short and long-wave radiation at the ocean surface and the sea surface temperatures (SST) allows the calculation of the radiative fluxes. The ocean currents are neglected in the calculation of the surface heat and momentum fluxes. Both the CRM and POM cover a horizontal domain of 512 km with 1 km grid spacing. The CRM has 50 levels with 100 m grid spacing near the surface, while POM has 58 levels with grid spacing of 2 cm to 5 m. Two different convective regimes during the TOGA–COARE intensive observing period (IOP) were simulated. The CRM was initialized with the average soundings over the COARE intensive flux area (IFA) on 00 UTC 07 December 1992 (Case 1) and 00 UTC 19 December 1992 (Case 2). The ocean model was initialized using data collected aboard the research vessel (R/V) Kexue No. 1 and the R/V Moana Wave. Similar to Grabowski et al (1996), forcing terms were added to certain prognostic equations of the CRM during the 9–10 day simulation periods to represent the large-scale tendencies of momentum, temperature and moisture in the CRM, but no such forcing was applied to the ocean model. The ocean model was affected by surface fluxes associated with gustiness beneath active cumulonimbus downdrafts. Moreover, the model simulated the formation of precipitation-produced, stable freshwater lenses at the top of the ocean mixed layer, with a variety of horizontal dimensions and lifetimes. The simulated fresh anomalies show realistic features, such as a positive correlation between salinity and temperature, the development of a ocean surface jet in the direction of the wind and, as a consequence, downwelling (upwelling) on its downwind (upwind) edge. Figure 1 illustrates a precipitating cloud producing a freshwater lenses.

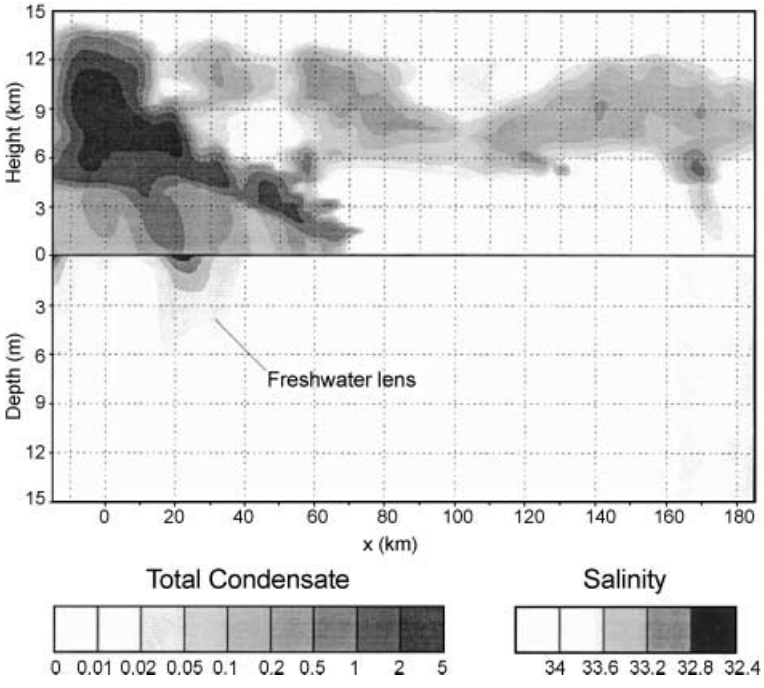


**Fig. 1.** A newly-formed freshwater lens and its parent storm at 19Z 22 December. The total condensate mixing ratio is shown in the upper panel (atmosphere) and the salinity field is depicted in the lower panel (ocean). The upper and lower panels have different vertical scales. [From Costa et al, 2001a]

### *4.4 Simulations of cumulonimbi and mesoscale convective systems*

Like most cloud-resolving modelers of cumulonimbi and mesoscale convective systems, in the past we have initialized RAMS with a horizontally-homogeneous single sounding and then perturbed that sounding with a temperature and/or moisture anomaly on the scale of a cloud updraft (Tripoli and Cotton, 1986; 1989a, b; Schmidt, 1995; Meyers, 1995; Grasso and Cotton, 1995). The resultant cloud simulations are somewhat idealized in that obtaining a ''representative sounding'' is always somewhat arbitrary and the cloud initiating mechanisms are by no means representative of the processes involved in the formation of actual clouds and cloud systems. For some storms such as rotating supercell storms, the simulated storm structure may not be very dependent on the actual cloud initiation mechanisms, but for others like ordinary cumulonimbi and small mesoscale convective systems (MCSs), the mechanism of cloud formation may have an important bearing on the structure, intensity, and evolution of the simulated storm.

Beginning with Grasso (1996), we began experimenting with simulations of cumulonimbi and MCSs in which RAMS is initialized more or less like a mesoscale forecast model in which synoptic data are analyzed and interpolated onto a coarse grid with grid spacing in the range of 50 to 75 km, actual terrain, land-use, soil type, soil moisture, and vegetation data are input into the surface model, and simulations are carried out for 12 to 36 h. During the simulation period, the lateral boundaries of the coarse grid are nudged with time-varying observed synoptic data. A number of refined grids are telescoped down to a grid spacing capable of explicitly resolving convective-scale motions, say 1 to 2 km. Generally three telescoping grids are used from the beginning of the simulation, and then near the time of observed storm formation, a cloud-resolving grid is spawned and then run for the duration of the simulation. Cloud initiation in these simulations is not done by introducing arbitrary perturbations of temperature and moisture, but instead form in response to mesoscale anomalies created by terrain gradients (Hertenstein, 1996; Nachamkin and Cotton, 2000, Chase et al, 1999), soil moisture and/or vegetation gradients driving dryline frontogenesis (Grasso, 1996; Ziegler et al, 1995; 1997; Shaw et al, 1997), land–sea thermal contrasts (Alexander and Cotton, 1998; Pielke et al, 1991b; Xian and Pielke, 1991; Nicholls et al, 1991a), cold pools produced by preexisting MCSs (Finley, 1997), cold fronts (Cram et al, 1992a, b) or some combination of those features. Pielke (2001c) summarizes the role of the spatial distribution of vegetation and soils on the prediction of cumulus convection rainfall, using examples from RAMS, and other models. Nicholls et al (1991b; 1993a) use RAMS to explore the role of thermally-forced gravity waves in the generation and propagation of cumulus convection.

Generally the decision of when and where to spawn the cloud-resolving grid is based on the development of rather crudely represented convection on Grid #3, having about 5 km grid spacing. Sometimes multiple storms are seen on Grid #3, but the cloud-resolving grid is either made big enough to encompass all those storms or is located where the most intense of the storms is located on Grid #3. In the most extreme use of nested grids, Grasso (1996) used a total of six interactive grids going from 75 km to 111 m grid spacing. In the case of the 26 April 1991 case, a F4/F5 tornado with maximum tangential wind speeds of 102 m/s and a 95 mb pressure drop was simulated. It is interesting that since then we have made several attempts to simulate the same intensity tornado using horizontally-homogeneous soundings derived from the simulated mesoscale environment prior to and near the location of the supercell storm. While moderate strength tornadoes were simulated, none reached the strength of the inhomogeneously initialized runs. The implication of this result is that the ultimate tornadic intensity in the inhomogeneously initialized run is achieved through convergence of environmental vorticity generated along the simulated dryline.

Using a model setup similar to Grasso, Finley (1997) also spawned six interactive nested grids, and for the 15 May 1991 case was not only able to simulate a moderate strength primary tornadic vortex, but also the formation of secondary vortices for a ten minute period during the 50 minute lifetime of the simulated tornado. Although rather poorly resolved with the 111 m fine grid

spacing, the simulated secondary vortices had many features in common with multiple vortex tornadoes and secondary vortices produced in the laboratory. In contrast to axisymmetric models, the secondary vortices formed on one side of the tornado and dissipated on the other side. While it has not been possible to conclusively identify the secondary vortex forcing mechanisms, it is noteworthy that they formed in a region of enhanced vertical and tangential velocities (and their gradients) where a downdraft wrapped cyclonically around the tornado vortex.

The MCS simulation by Nachamkin and Cotton (2000) was remarkable in that it closely resembled the radar observed bow-echo appearance of the storm, the locations of the strongest cells, and the overall morphological evolution of the storm. Of course, this was facilitated by strong terrain forcing in the region, which produced two interacting transverse topographically-induced thermally-driven, solenoids and a pre-existing surface front that were instrumental in generating the MCS. As observed, the MCS intensified further east when it intercepted an intense low-level jet (LLJ) of $< 200$ km width. The LLJ formed due to an initial west–east soil moisture gradient and an associated variation in boundary layer depth.

In another MCS simulation, Bernardet and Cotton (1998) simulated the evolution of an afternoon squall line into a derecho-producing nocturnal MCS. Derechos are convectively-produced windstorms with durations of 8 hours or more. Severe winds associated with this event occurred between 0600 and 1200 UTC on 13 May 1985, and was preceded by afternoon convection in the form of a squall line on 12 May 1985. RAMS was initialized with NCEP data enhanced with soundings and surface observations. Four telescopically nested grids covering the synoptic scale down to the cloud scale were used, with the finest grid having 2 km spacing. A 24-hour simulation was performed starting at 1200 UTC 12 May 1985. During the day, when the boundary layer was well mixed, a squall line formed in which the source of air for the clouds was located within the boundary layer, near the ground. At night, when the boundary layer became stable, the source of air shifted to the top of the boundary layer and was composed of warm, moist air transported by the nocturnal LLJ.

During the night, downdrafts were stronger, generating strong surface winds. The most important branch of the nocturnal downdraft has an ''up-down'' trajectory. The upward pressure gradient force is partially related to mid-level rotation in the storm, which has characteristics of a high-precipitation supercell. The outflow of this negatively-buoyant downdraft near the ground is responsible for the formation of severe surface winds.

### *4.5 Simulations of hurricanes*

Multiple nested grid simulations of hurricanes have been carried out with a fine grid resolution capable of explicitly resolving convection within the hurricane core. Nicholls and Pielke (1995) conducted idealized simulations of hurricane development in horizontally homogeneous environments. A fine grid with an increment of 4 km and a width of 360 km was embedded in two successively coarser resolution grids. The width of the coarsest grid was 2100 km. The simulation was initialized using an Atlantic hurricane season sounding (Jordan, 1958), and a deep cyclonic vortex in gradient wind balance. The maximum wind speed of the vortex was 20 m/s at a radius of 40 km from the center. Over a period of 30 h a hurricane rapidly developed with a realistic structure that included spiral bands, a clear eye and a radius of maximum winds that sloped with height. These idealized simulations suggest that in the absence of shear a tropical storm over warm water can undergo rapid intensification without any environmental forcing being necessary. Interesting oscillations of the total mass of liquid and ice water in the domain occurred with a period of a few hours. The causes of these oscillations and the implications of the associated latent heating rate changes on structure and intensification are interesting topics for future research.

Eastman (1995) carried out a simulation of Hurricane Andrew with RAMS, which was initialized using NMC gridded pressure data, upper air rawinsonde data observations, and a bogus vortex in gradient wind balance. The storm was initialized at 12 UTC on 21 August 1992, three days prior to landfall. During the first 36 h the simulated storm underwent rapid intensification in agreement with observations and the track was

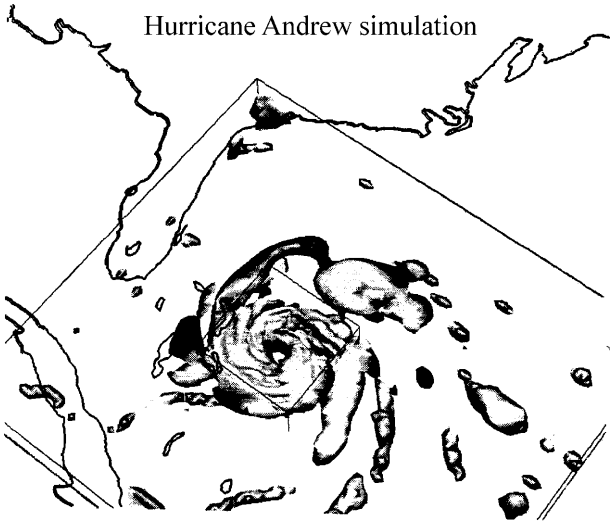


**Fig. 2.** Perspective view of hurricane Andrew from the southeast, shown at 66 hours simulation time. The shaded isosurface is condensate mixing ratio set to 1.9 g/kg. Only the 20 km and 5 km grids are shown, with the grid boundaries outlined. [From Eastman, 1995]

very similar to that of the observed storm. Subsequently, the simulated model solution began to diverge from the observations as it tracked towards the northwest while the observations showed the cyclone stayed on a westerly course. Figure 2 is a three-dimensional rendering of the tropical cyclone. The gray-scaled field represents an isosurface of total condensate mixing ratio, set to 0.1 g/kg, taken 60 h into the simulation. A banded structure can be seen, with several bands extending outside the finest mesh. An eye is also evident with a diameter of 60 km at this time. The simulated hurricane made landfall in central Florida rather than southern Florida, but nevertheless this was fairly good agreement considering the model was integrated for more than three days of simulation time.

The Third Convection and Moisture Experiment (CAMEX-3) was carried out during the 1998 hurricane season. The goal of the program was to improve hurricane and tropical storm prediction and increase the understanding of these systems. High-resolution measurements within Hurricane Bonnie were obtained during the field campaign. RAMS was exercised to gauge the impact of high-resolution wind and moisture observations from dropsondes and Lidar Atmospheric Sensing Experiment (LASE) water vapor profiles on storm track and intensity prediction (Nicholls et al, 2000). A control simulation was initialized using NCEP reanalysis data and sensitivity tests were then carried out to investigate the impact of including the CAMEX-3 data. The track forecast was improved when the high-resolution data was included. The study did, however, point out a limitation of the dropsonde data coverage as far as model initialization is concerned, since it was too localized to provide sufficient details of the vortex structure. This resulted in unrealistic asymmetries of the analyzed wind field about the vortex center.

### *4.6 Extreme precipitation estimation*

Building on successful simulations of flash flood events with RAMS by Nair et al (1997), and Abbs (1999), we have been performing simulations of historical flood cases in Colorado. The ultimate aim of this research is to develop new methodologies of extreme precipitation estimation derived in part from those simulations. At least 20 historical cases have been selected from the various hydroclimatic regions identified by Doesken and McKee (1998; see Fig. 3). Besides the basic control simulations, we are developing a systematic methodology for perturbing initial conditions for the simulations. The parameter space used to define those perturbations is extracted from soundings representative of the climatology of extreme rainfall events over Colorado during the period covered by the NCEP reanalyses (roughly since 1957). The methodology resembles ensemble forecast strategy except that the parameter space is purposely skewed toward extreme rainfall events. Another technique being used is to shift the observed synoptic fields for an observed extreme precipitation event relative to the topography, in an effort to artificially increase the sample size beyond the limited number of observed events. These synoptically shifted simulations show how synoptic settings identical to those observed in extreme precipitation cases, except for their displacement, might impact various regions around Colorado.

To date, we have performed numerous simulations of the 28 July 1997 Fort Collins, CO flash flood event (Petersen et al, 1999) in which the locations and amount of rainfall were found to be dependent upon the method of soil moisture estimation (Ashby, 2001). Several runs with shifted synoptic patterns relative to the mountainous

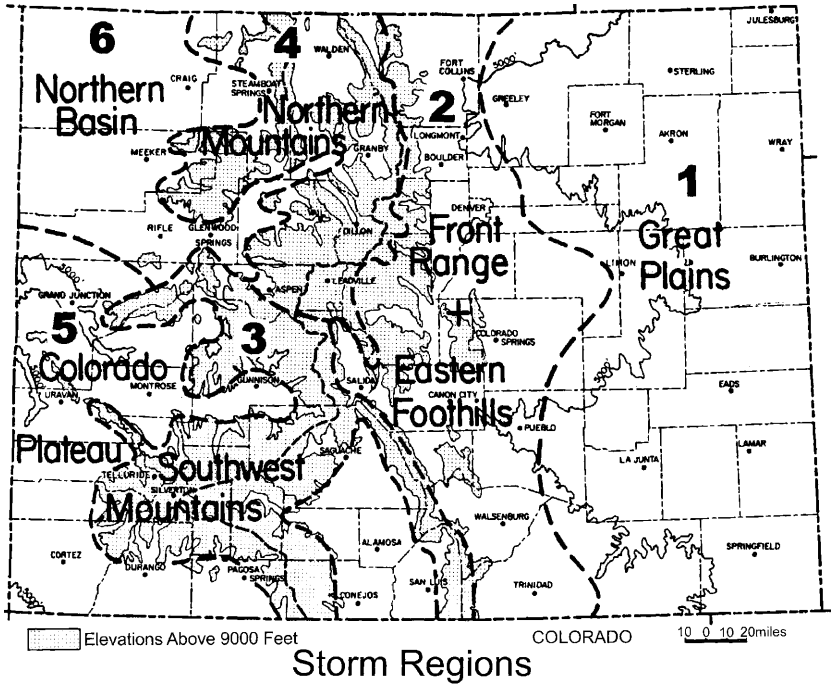


**Fig. 3.** Approximate hydroclimatic regions of Colorado used to describe and characterize extreme precipitation events. [From Doesken and McKee, 1998]

terrain were also performed as well as an initial control simulation of a case in southwestern Colorado on 4–6 September 1970. In the latter case, a stream of moisture from an eastern Pacific tropical storm fed into the southwestern U.S. as a baroclinic system dug into the Great Basin, with widespread flood-producing rains in Arizona, southwestern Colorado and southeastern Utah. Four interactive nested grids were used, with horizontal grid spacing ranging from about 80 km to $\sim 2$ km, and with the finest or cloud-resolving grid domain being about 150 to 250 km in its horizontal dimensions. The model was able to simulate the regions of extreme precipitation well, as well as the altitudes of transition from rain to graupel/hail precipitation.

### *4.7 Climate applications*

Pielke (1998), and Pielke (2001a) concluded that realistic simulations of seasonal and longer-term weather requires that earth surface-atmosphere feedbacks be included. These integrative model simulations are, therefore, more appropriately called climate simulations.

In order to provide monthly and seasonal RAMS simulations, RAMS has been generalized to permit longer-term calculations (Copeland et al, 1996; Pielke et al, 1997; 1999c; Liston and Pielke, 2001). A comparison of the ability to simulate seasonal weather is reported in Takle et al (1999). The components of the model that were added in Liston and Pielke (2001) include: (1) the changes over time of the solar declination; (2) sea-surface temperatures and vegetation parameters are updated daily; (3) a moisture- and precipitation-physics scheme for long model runs are implemented; and (4) simplified incoming shortwave and longwave radiation schemes are introduced. In addition, a more general analysis package for output variables was implemented.

In the Liston and Pielke (2001) paper, the model was integrated for a season with the fine grid nested over the central Great Plains (with 50 km horizontal grid lengths) for 1989, and the resulting precipitation and temperatures compared at specific locations and averaged over the domain. This version of the RAMS model (which has been referred to as ClimRAMS) was also applied in the PIRC (Project for Intercomparison of Regional Climate) model study (Takle et al, 1999).

ClimRAMS has also been coupled to two biogeochemical models (CENTURY; Lu et al, 2001, and GEMTM; Eastman et al, 2001a). In the ClimRAMS–CENTURY coupling, the atmospheric model is integrated for a week, and the precipitation and temperature data fed into the biogeochemical model. The plants ''grow'' in

that model and new leaf area index (LAI) values returned to the atmospheric model, where the new LAI values are used in the surface flux calculations. In the Lu et al (2001) paper, this coupled system was also applied to the central Great Plains for 1989. Among the results, it was concluded that the incorporation of dynamic vegetation growth into seasonal weather prediction was important and necessary if more accurate predictions are to be achieved.

The ClimRAMS–GEMTM coupling is more intimate in that both models exchange information on the same time step (around 120 seconds for the Eastman et al, 2001a paper). This coupled system was applied to the Great Plains for 1989 where the validation included both atmospheric quantities such as temperature and precipitation, as well the land surface variable LAI. Sensitivity experiments with the coupled models also demonstrated that, for seasonal time scales and over this region, the biogeochemical effect of increased $CO_2$ on weather would have a much more significant effect than the radiative effect of increased $CO_2$. The conversion of the natural landscape in the region to the current landscape was also shown to have had a major effect on seasonal weather in the central Great Plains. Eastman et al (2001b) has recently demonstrated using these coupled models that grazing by tens of millions of bison in the period before European settlement also significantly affected the weather in this region. Work continues with the two-coupled models to study longer time periods and other geographic locations. This version of RAMS has also been applied to investigate the relation between landscape, snow cover depletion and regional weather (Greene et al, 1999).

### *4.8 Prototype realtime forecasting with RAMS*

At Colorado State University RAMS has been used for real-time forecasting since 1991 (Cotton et al, 1994; http://rams.atmos.colostate.edu/cases/). The feasibility of using RAMS as a forecast model has been investigated also by Snook and Pielke (1995), Mukabana and Pielke (1996), and Papineau et al (1994). Originally a simple ''dump-bucket'' scheme (Cotton et al, 1995) was used to generate quantitative precipitation forecasts (QPF), but starting in the fall of 1995 real-time forecasts used the bulk microphysics scheme available with RAMS. Gaudet and Cotton (1998) showed that the bulk microphysics improved the forecasting of the areal extent and maximum amount of precipitation, especially when compared to the snow telemetry (SNOTEL) automatic pillow-sensor stations, which are found at locations more representative of the model topography. For the month of April 1995, a series of 24-hour accumulated precipitation forecasts was generated with both the dump-bucket and microphysics versions of the forecast model. Both sets of output were compared to a set of 167 community-based station reports, and to a set of 32 SNOTEL stations. Climatological station precipitation forecasts were improved on the average by correcting for the difference between a station's actual elevation and the cell-averaged topography used by the model. The model had more problems with the precise timing and geographical location of the precipitation features, probably due in part to the influence of other model physics, the failure of the model to resolve adequately winter-time convection events, and lack of mesoscale detail in the initializations.

The current prototype realtime forecast version of RAMS at CSU is based on version 4.29. The model is set up on a 21-processor cluster of 450 MHz Pentium PCs. Two configurations are run daily. The first is the standard meteorological forecast model configuration that has three interactive nested grids. Grid #1 has 48 km grid spacing and covers the entire U.S. (see Fig. 4), Grid #2 has 12 km grid spacing and covers all of Colorado, most of Wyoming, and portions of adjacent states, and Grid #3 has 3 km grid spacing covering a 150 km × 150 km area that is relocatable anywhere within Grid #2. Vertical grid spacing on all grids starts with 150-km spacing at the lowest levels and is stretched to 1000 m aloft, with a total of 36 vertical levels extending into the stratosphere. The model is initialized with 00 UTC ETA model analysis fields and run for a period of 48 h, with the lateral boundary region of the coarse grid nudged to the ETA 6-hourly forecast fields. A 48 h run takes about 4 h of CPU. We are currently assessing the value added to the forecasts using the 3 km grid. Preliminary analysis suggests that the model is able to forecast the formation and propagation of individual convective storms,

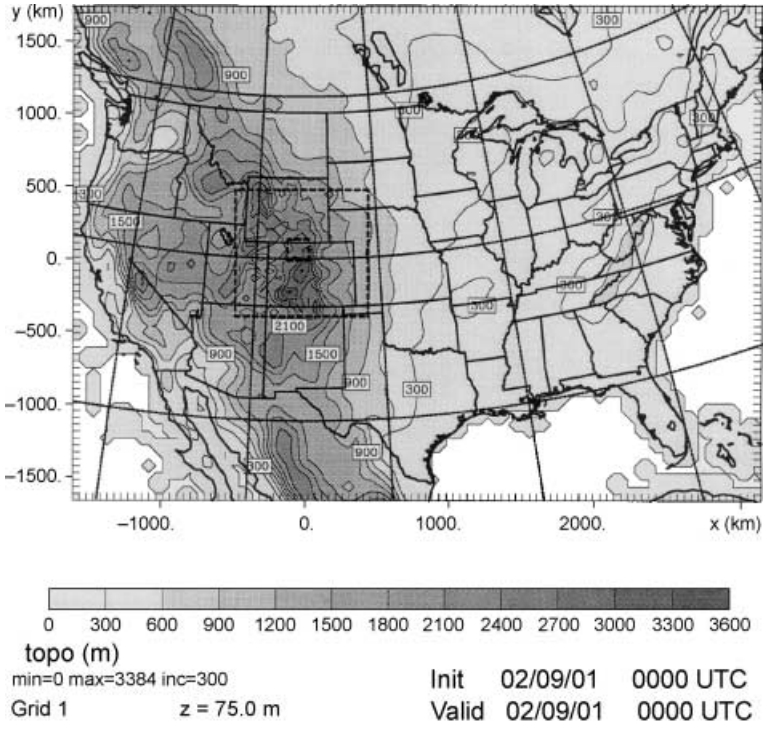


**Fig. 4.** Grid setup for realtime forecast version of RAMS. Entire Grid #1 domain is shown, with topography contoured. Nested Grids #2 and #3 domains are indicated as dashed boxes in the Colorado Rocky Mountain region

especially those originating in the mountains, and severe downslope windstorm events (see Cotton et al, 1995). The model exhibits a consistent over-prediction bias on precipitation. We are currently seeking the source of that bias and hope to rectify that shortly. Although ''false alarms'' of precipitation events are forecast, they occur relatively rarely.

The second prototype forecast model emphasizes boundary layer forecast applications. In this configuration Grid #1 is the same as the standard forecast model. Grid #2 is similarly configured as well, except that it and Grid #3 can be relocated anywhere in the continental U.S. Grid #3 has vertically nested levels with 50 m spacing to 1 km and 75 m spacing to 1.5 km, and covers a 150 km × 150 km area with 3 km horizontal spacing. This version is initialized with 1200 UTC ETA model analysis fields and is also nudged to ETA forecast boundaries for a 48 h period. The aim of this forecast cycle is to provide high-resolution, accurate forecasts of boundary layer winds, temperature, moisture, turbulence (using the Mellor and Yamada (1974) level 2.5 TKE scheme), and other specialized products. One such product we jokingly call the Cotton Soaring Index (CSI), see Fig. 5. This product is available on all RAMS forecast grids. It uses model surface forecast temperatures and then calculates the difference between forecast air temperatures 1600 m above the local grid point ground level and the temperature of a parcel lifted dry adiabatically to that level. Like the lifted index, the more negative the value of CSI, the better the potential for finding good thermals for soaring gliders. The height of 1600 m AGL is chosen because it is high enough above ground level to permit safe cross-country flights in gliders. Other model products useful to soaring forecasting are vertical cross sections of TKE (giving boundary layer depth variablility over terrain), cloud base heights, winds, and precipitation. Relocatable grid operations with this model have been tested over the Whitesands Missile Range, near Littlefield, TX in support of a Soaring Society of America regional forecast contest, Tucson, AR, to support Dr. Cotton's glider flights in the area, in the vicinity of the WLEF Tower, WI in support of $CO_2$ Budget and Rectification Airborne Study (COBRA) at various locations in Colorado, southern Minnesota, and near Leon, Kansas in support of the CASES-99 field experiment (see website: http://www.colorado-research.com/cases/CASES-99.html). Detailed evaluations of the boundary forecast model is underway using data acquired during CASES-99.

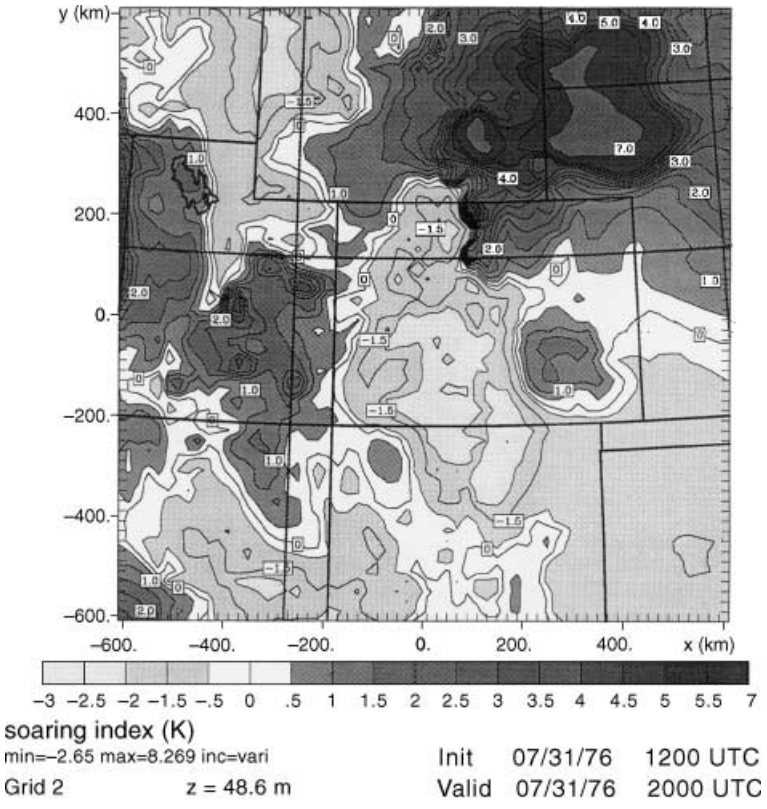


**Fig. 5.** Early afternoon forecast of the Cotton Soaring Index. Areas with values below − 0.5 K are conducive to thermals and are contoured with lighter shades. Areas with values above 0.5 K are stable and are contoured with darker shades

### *4.9 Modeling airflow around buildings*

With suitable boundary conditions for walls and roofs (Nicholls et al, 1993b) RAMS has been applied to the simulation of airflow around buildings. Figure 6 shows a horizontal cross-section of streamlines near the surface for flow around a cubic building, with 60 grid points along a side and a grid increment of 1 m. For this simulation, the incident flow is at an oblique angle to the building and is fully turbulent. An oblique incident flow is of particular interest since corner conical vortices develop on top of the roof and are associated with strong wind loads near the upwind corner (Peterka and Cermak, 1976). The model was able to successfully simulate the development of corner conical vortices (Nicholls et al, 1993c; Pielke and Nicholls, 1997) and the shape of the pressure field on top of the roof was similar to that obtained from wind tunnel experiments (Peterka et al, 1996).

As an example of the application of multiple nested grids to span a wide range of spatial scales, Nicholls et al (1993c) conducted a two-dimensional simulation of a microburst-producing thunderstorm and the resultant airflow

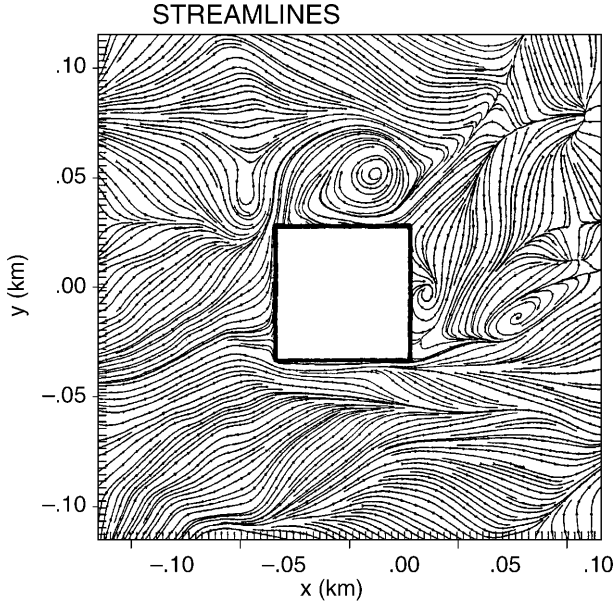


**Fig. 6.** Horizontal cross-section of streamlines near the surface for flow around a cubic building. [From Nicholls et al, 1993b]

around a building. A storm was initialized using the 2300 UTC 2 August 1985 Dallas-Ft. Worth, Texas microburst sounding used by Proctor (1989). Only the coarsest grid was activated

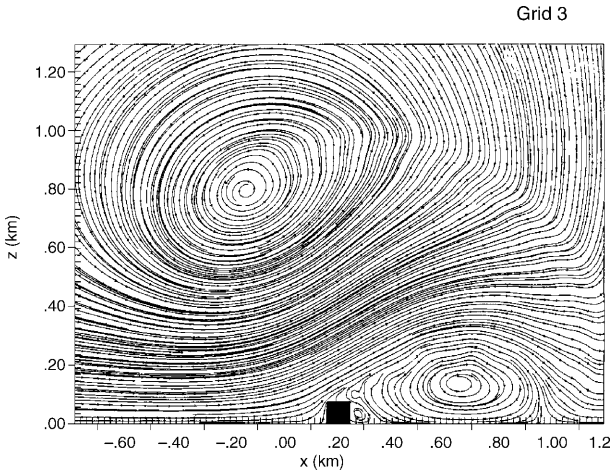


**Fig. 7.** Vertical cross-section of streamlines in grid 3, showing the flow around a building produced by a microburst. [From Nicholls et al, 1993c]

during the development stage of the convective storm. When the convective storm generated a microburst the four finer scale grids were activated, with the building situated in the center of the finest grid. The microburst propagated into the finer grids enabling the small-scale flow around the building to be investigated. Figure 7 shows the streamlines at $t = 5400$ s for grid 3. This shows the microburst vortex centered at a height of 0.8 km and a smaller clockwise rotating vortex that has been shed from the building. There are two finer grids which further ''telescope down'' in scale showing more detail of the separation of the flow at the windward corner of the building and the formation of vortices (not shown).

The application of the shaved coordinate scheme will permit simulations of flow of air around more complex building shapes and be investigated in the future.

### *4.10 Air pollution applications*

RAMS has been used in a wide variety of air pollution studies. In most of these applications, RAMS simulated winds and turbulence are inserted into a Lagrangian dispersion model, as described in Uliasz et al (1996). Examples of these RAMS applications include Lyons et al (1992; 1995), Pielke et al (1992b), Moran and Pielke (1996a, b), Kallos et al (1993), Eastman et al (1995), Poulos and Pielke (1994), and Pielke and Uliasz (1998).

## 5. Conclusion

We have described some of the main features of RAMS as it has evolved from its origins as a cloud model and two hydrostatic mesoscale models. We have also described some of the applications of the model, which range from synoptic scale weather systems and climate studies down to large eddy simulations and even flow around urban buildings. RAMS is a continually evolving modeling system that is now moving to full global scale simulations for both climate and forecasting applications. Further advances in physics algorithms are also under development, which should improve the simulation capabilities of the model for a variety of applications.

#### Acknowledgments

The authors would like to thank Brenda Thompson for assistance with word processing, reference citation gathering, and technical editing of this manuscript. This research was supported by the following agencies: The National Science Foundation under grants ATM-9900929, ATM-9904128 and ATM-9910857, Colorado Department of Natural Resources under contract ENC #C154213, the National Aeronautics and Space Administration under grants NAG-1-2045, NAG5-7560 and NAG8-1511, the National Oceanic and Atmospheric Administration under grant NA67RJ0152, the Colorado Agricultural Experiment Station under grant COL00692, the U.S. Department of Defense Center for Geosciences under contract DAAL01-98-2-0078, and United States Geological Survey under Contract No. 99CRAG005 SA 9005CS0014.

#### References

Abbs DJ (1999) A numerical modeling study to investigate assumptions used in the calculation of probable maximum precipitation. Water Res Res 35: 785–796

Alexander GD, Cotton WR (1998) The use of cloud-resolving simulations of mesoscale convective systems to build a convective parameterization scheme. J Atmos Sci 55: 408–419

Ashby T (2001) Impact of soil moisture initialization on a simulated flash flood. M.S. Thesis, Colorado State University, Department of Atmospheric Science, Fort Collins, CO 80523 (in preparation)

Band LE (1993) Effect of land surface representation on forest water and carbon budgets. J Hydrol 150: 749–772

Benjamin SG, Brewster KA, Brummer R, Jewett BF, Schlatter TW, Smith TL, Stamus PA (1991) An isentropic three-hourly data assimilation system using ACARS aircraft observations. Mon Wea Rev 119: 888–906

Bernardet LR, Cotton WR (1998) Multi-scale evolution of a derecho-producing MCS. Mon Wea Rev 126: 2991–3015

Blumberg AF, Mellor GL (1987) A description of a three-dimensional coastal ocean circulation model.

In: Three-dimensional coastal ocean models (Heaps NS, ed). Washington, DC: American Geophysical Union, pp 1–16

Cavalieri DJ (1992) Sea ice algorithm in NASA sea ice validation program for the Defense Meteorological Satellite Program Special Sensor Microwave Imager: Final Report, NASA Technical Memorandum 104559, pp 25–32

Chase TN, Pielke RA Sr, Kittel TGF, Baron JS, Stohlgren TJ (1999) Potential impacts on Colorado Rocky Mountain weather due to land use changes on the adjacent Great Plains. J Geophys Res 104: 16673–16690

Chen C, Cotton WR (1983) A one-dimensional simulation of the stratocumulus-capped mixed layer. Bound-Layer Meteor 25: 289–321

Chen C, Cotton WR (1987) The physics of the marine stratocumulus-capped mixed layer. J Atmos Sci 44: 2951–2977

Chen F, Pielke RA Sr, Mitchell K (2001) Development and application of land-surface models for mesoscale atmospheric models: Problems and promises. In: Observation and modeling of the land surface hydrological processes (Lakshmi V, Alberston J, Schaake J, eds). American Geophysical Union (forthcoming)

Cheng WYY, Wu T, Cotton WR (2001) Large-eddy simulations of the 26 November, 1991 FIRE II cirrus case. J Atmos Sci (forthcoming)

Cooper WA (1980) A method of detecting contact ice nuclei using filter samples. Preprints, 8th Int. Conf. on Cloud Physics, Clermont-Ferrand, France, pp 665–668

Copeland JH, Pielke RA Sr, Kittel TGF (1996) Potential climatic impacts of vegetation change: A regional modeling study. J Geophys Res 101: 7409–7418

Costa AA, Cotton WR, Walko RL, Pielke RA Sr (2001a) Coupled ocean–cloud-resolving simulations of the air–sea interaction over the equatorial western Pacific. J Atmos Sci (submitted)

Costa AA, Cotton WR (2001b) Long term numerical simulations of the western Pacific coupled system. J Atmos Sci (submitted)

Cotton WR, Tripoli GJ, Rauber RM, Mulvihill EA (1986) Numerical simulation of the effects of varying ice crystal nucleation rates and aggregation processes on orographic snowfall. J Clim Appl Meteor 25: 1658–1680

Cotton WR, Thompson G, Mielke PW Jr (1994) Real-time mesoscale prediction on workstations. Bull Amer Meteor Soc 75: 349–362

Cotton WR, Weaver JF, Beitler BA (1995) An unusual summertime downslope wind event in Fort Collins, Colorado on 3 July, 1993. Wea Forecast 10: 786–797

Cram JM, Pielke RA, Cotton WR (1992a) Numerical simulation and analysis of a prefrontal squall line. Part I: Observations and basic simulation results. J Atmos Sci 49: 189–208

Cram JM, Pielke RA, Cotton WR (1992b) Numerical simulation and analysis of a prefrontal squall line. Part II: Propagation of the squall line as an internal gravity wave. J Atmos Sci 49: 209–225

Davies HC (1983) Limitations of some common lateral boundary schemes used in regional NWP models. Mon Wea Rev 111: 1002–1012

DeMott PJ, Meyers MP, Cotton WR (1994) Parameterization and impact of ice initiation processes relevant to numerical model simulations of cirrus clouds. J Atmos Sci 51: 77–90

Deshler T (1982) Contact ice nucleation by submicron atmospheric aerosols. PhD Dissertation, Department of Physics and Astronomy, University of Wyoming, Laramie, WY, 107 pp

Doesken NJ, McKee TB (1998) An analysis of rainfall for the July 28, 1997 flood in Fort Collins, Colorado. Climatology Report 98-1, Colorado Climate Center, Department of Atmospheric Science, Colorado State University, Fort Collins, CO 80523-1371, 55 pp

Eastman JL (1995) Numerical simulation of hurricane Andrew – Rapid intensification. 21st Conf. on Hurricanes and Tropical Meteorology, Miami, Florida

Eastman JL, Pielke RA, Lyons WA (1995) Comparison of lake-breeze model simulations with tracer data. J Appl Meteor 34: 1398–1418

Eastman JL, Pielke RA, McDonald DJ (1998) Calibration of soil moisture for large eddy simulations over the FIFE area. J Atmos Sci 55: 1131–1140

Eastman JL, Coughenour MB, Pielke RA (2001a) The effects of $CO_2$ and landscape change using a coupled plant and meteorological model. Glob Change Biol (forthcoming)

Eastman JL, Coughenour MB, Pielke RA (2001b) Does grazing affect regional climate. J Hydrometeorol (forthcoming)

Elder K, Dozier J, Michaelsen J (1991) Snow accumulation and distribution in an alpine watershed. Water Res Res 27: 1541–1552

Feingold G, Stevens B, Cotton WR, Frisch AS (1996) The relationship between drop in-cloud residence time and drizzle production in numerically simulated stratocumulus clouds. J Atmos Sci 53: 1108–1122

Feingold G, Walko RL, Stevens B, Cotton WR (1998) Simulations of marine stratocumulus using a new microphysical parameterization scheme. Atmos Res 47–48: 505–528

Feingold G, Cotton WR, Kreidenweis SM, Davis JT (1999) The impact of giant cloud condensation nuclei on drizzle formation in stratocumulus: Implications for cloud radiative properties. J Atmos Sci 56: 4100–4117

Finley CA (1997) Numerical simulation of intense multiscale vortices generated by supercell thunderstorms. PhD Diss., Colorado State University, Department of Atmospheric Science, Fort Collins, CO 80523, 297 pp

Flato GM, Hibler III WD (1995) Ridging and strength in modeling the thickness distribution of Arctic sea ice. J Geophys Res 100: 18611–18626

Fletcher NH (1962) Physics of rain clouds. London: Cambridge University Press

Frank WM, Cohen C (1987) Simulation of tropical convective systems, Pt. 1: Cumulus parameterization. J Atmos Sci 44: 3787–3799

Gaudet B, Cotton WR (1998) Statistical characteristics of a real-time precipitation forecasting model. Wea Forecast 13: 966–982

Grabowski WW, Wu X, Moncrieff MW (1996) Cloud-resolving modeling of tropical cloud systems during phase III of GATE. Part I: Two-dimensional experiments. J Atmos Sci 53: 3684–3709

Grasso L (1996) Numerical simulation of the May 15 and April 26, 1991 tornadic thunderstorms. Atmos Sci Paper #596, Colorado State University, Department of Atmospheric Science, Fort Collins, CO 80523, 151 pp

Grasso LD, Cotton WR (1995) Numerical simulation of a tornado vortex. J Atmos Sci 52: 1192–1203

Greene EM, Liston GE, Peilke RA Sr (1999) Relationships between landscape, snowcover depletion, and regional weather and climate. Hydrol Proc 13: 2453–2466

Hadfield MG, Cotton WR, Pielke RA (1991) Large-eddy simulations of thermally-forced circulations in the convective boundary layer. Part I: A small-scale circulation with zero wind. Bound-Layer Meteor 57: 79–114

Hadfield MG, Cotton WR, Pielke RA (1992) Large-eddy simulations of thermally forced circulations in the convective boundary layer. Part II: The effect of changes in wavelength and wind speed. Bound-Layer Meteor 58: 307–328

Harrington JY (1997) The effects of radiative and microphysical processes on simulated warm and transition season Arctic stratus. PhD Diss., Atmospheric Science Paper No 637, Colorado State University, Department of Atmospheric Science, Fort Collins, CO 80523, 289 pp

Harrington JY, Meyers MP, Walko RL, Cotton WR (1995) Parameterization of ice crystal conversion processes due to vapor deposition for mesoscale models using double-moment basis functions. Part I: Basic formulation and parcel model results. J Atmos Sci 52: 4344–4366

Harrington JY, Reisin T, Cotton WR, Kreidenweis SM (1999) Cloud resolving simulations of Arctic stratus. Part II: Transition-season clouds. Atmos Res 55: 45–75

Harrington JY, Feingold G, Cotton WR, Kreidenweis SM (2000) Radiative impacts on the growth of a population of drops within simulated summertime Arctic stratus. J Atmos Sci 57: 766–785

Harrington JY, Olsson PQ (2001a) A method for the parameterization of cloud radiative properties within numerical models. Implications for Arctic cloudy boundary layers. Atmos Res (forthcoming)

Harrington JY, Olsson PQ (2001b) Numerical simulations of the influence of ice nuclei on strongly surface forced mixed-phase stratocumulus cloud dynamics. J Geophys Res (submitted)

Harrington JY, Olsson PQ (2001c) An LES study of the influence of ice microphysics on roll cloud dynamics and structure over the marginal ice zone. Preprints, 6th Conf. on Polar Meteorology and Oceanography, 14–18 May, San Diego, California

Heckman ST, Cotton WR (1993) Mesoscale numerical simulation of cirrus clouds – FIRE case study and sensitivity analysis. Mon Wea Rev 121: 2264–2284

Hertenstein RFA (1996) Evolution of potential vorticity associated with mesoscale convective systems. PhD Diss., Colorado State University, Department of Atmospheric Science, Fort Collins, CO 80523, 170 pp. (Available as Atmospheric Science Paper No 599.)

Hill GE (1974) Factors controlling the size and spacing of cumulus clouds as revealed by numerical experiments. J Atmos Sci 31: 646

Hobbs PV, Rangno AL (1985) Ice particle concentrations in clouds. J Atmos Sci 42: 2525–2549

Hodur RM (1997) The Naval Research Laboratory's Coupled Ocean/Atmosphere Mesoscale Prediction System (COAMPS). Mon Wea Rev 125: 1414–1430

Hudson JG (1989) An instantaneous CCN spectrometer. J Atmos Ocean Tech 6: 1055–1065

Hunke EC, Lipscomb WH (1999) CICE: The Los Alamos sea-ice model, documentation and software, vers. 2.0, Los Alamos National Laboratory, LA-CC-98-16, v.2

Jiang H, Cotton WR (2000) Large-eddy simulation of shallow cumulus convection during BOMEX: Sensitivity to microphysics and radiation. J Atmos Sci 57: 582–594

Jiang H, Cotton WR, Pinto JO, Curry JA, Weissbluth MJ (2000) Cloud resolving simulations of mixed-phase Arctic stratus observed during BASE: Sensitivity to concentration of ice crystals and large-scale heat and moisture advection. J Atmos Sci 57: 2105–2117

Jiang H, Feingold G, Cotton WR, Duynkerke PG (2001) Large-eddy simulations of entrainment of cloud condensation nuclei into the Arctic boundary layer: 18 May, 1998 FIRE/SHEBA case study. J Geophys Res 106: 15,113–15,122

Jordan CL (1958) Mean soundings for the West Indies area. J Meteor 15: 91–97

Kallos G, Kassomenos P, Pielke RA (1993) Synoptic and mesoscale weather conditions during air pollution episodes in Athens, Greece. Bound-Layer Meteor 62: 163–184

Kessler E (1969) On the distribution and continuity of water substance in atmospheric circulations. Meteor Monogr 32, Amer Met Soc, pp 1–84

Klemp JB, Wilhelmson RB (1978) The simulation of three-dimensional convective storm dynamics. J Atmos Sci 35: 1070–1096

Kosovic B (1997) Subgrid scale modeling for the large-eddy simulation of high-Reynolds-number boundary layers. J Fluid Mech 336: 151–182

Lee TJ, Pielke RA, Mielke PW Jr (1995) Modeling the clear-sky surface energy budget during FIFE87. J Geophys Res 100: 25585–25593

Lilly DK (1962) On the numerical simulation of buoyant convection. Tellus XIV: 148–172

Lipscomb WH (2000) Remapping the thickness distribution of sea ice. J Geophys Res 106: 13989

Liston GE (1995) Local advection of momentum, heat, and moisture during the melt of patchy snow covers. J Appl Meteor 34: 1705–1715

Liston GE (1999) Interrelationships among snow distribution, snowmelt, and snow cover depletion: Implication for atmospheric, hydrologic, and ecologic modeling. J Appl Meteor 38: 1474–1487

Liston GE (2001) Modeling subgrid snowcover heterogeneities in regional and global weather, climate, and hydrologic models. J Clim (submitted)

Liston GE, Pielke RA Sr (2001) A climate version of the regional atmospheric modeling system. Theor Appl Climatol 68: 155–173

Liston GE, Sturm M (1998) A snow-transport model for complex terrain. J Glaciol 44: 498–516

Liston GE, Pielke RA Sr, Greene EM (1999) Improving first-order snow-related deficiencies in a regional climate model. J Geophys Res 104: 19559–19567

Lu L (1999) Implementation of a two-way interactive atmospheric and ecological model and its application to the central United States. PhD Diss., Colorado State University, Department of Atmospheric Science, 134 pp

Lu L, Pielke RA, Liston GE, Parton WJ, Ojima D, Hartman M (2001) Implementation of a two-way interactive atmospheric and ecological model and its application to the central United States. J Clim 14: 900–919

Lyons WA, Pielke RA, Cotton WR, Keen CS, Moon DA, Lincoln NR (1992) Some considerations of the role of the land/lake breeze in causing elevated ozone levels in the southern Lake Michigan region. In: Environmental Modeling (Melli P, Zannetti P, eds), chap. 9. Southampton: Computational Mechanics Publications, pp 51–171

Lyons WA, Tremback CJ, Pielke RA (1995) Applications of the Regional Atmospheric Modeling System (RAMS) to provide input to photochemical grid models for the Lake Michigan Ozone Study (LMOS). J Appl Meteor 34: 1762–1786

Mace GG, Starr DO'C, Ackerman TP, Minnis P (1995) Examination of coupling between an upper-tropospheric cloud system and synoptic-scale dynamics diagnosed from wind profiler and radiosonde data. J Atmos Sci 5: 4094–4127

Mahrer Y, Pielke RA (1977) A numerical study of the airflow over irregular terrain. Beiträge zur Physik der Atmosphäre 50: 98–113

Maykut GA, Understeiner N (1971) Some results from a time dependent thermodynamic model of sea ice. J Geophys Res 76: 1550–1575

McCumber M (1980) A numerical simulation of the influence of heat and moisture fluxes upon mesoscale circulations. PhD Diss., Department of Physics, University of Virginia, 277 pp

McCumber MC, Pielke RA (1981) Simulation of the effects of surface fluxes of heat and moisture in a mesoscale numerical model. Part I: Soil layer. J Geophys Res 86: 9929–9938

Mellor GL, Yamada T (1974) A hierarchy of turbulence closure models for planetary boundary layers. J Atmos Sci 31: 1791–1806

Mellor GL, Yamada T (1982) Development of a turbulence closure model for geophysical fluid problems. Rev Geophys Space Phys 20: 851–875

Meyers MP (1995) The impact of a two-moment cloud model on the microphysical structure of two precipitation events. PhD Diss., Colorado State University, Department of Atmospheric Science, Fort Collins, CO 80523-1371, 165 pp. (Available as Atmospheric Science Paper #575.)

Meyers MP, DeMott PJ, Cotton WR (1992) New primary ice nucleation parameterizations in an explicit cloud model. J Appl Meteor 31: 708–721

Meyers MP, Walko RL, Harrington JY, Cotton WR (1997) New RAMS cloud microphysics parameterization. Part II: The two-moment scheme. Atmos Res 45: 3–39

Mitrescu C (1998) Cloud-resolving simulations of tropical cirrus clouds. MS Thesis, Colorado State University, Department of Atmospheric Science, Fort Collins, CO 80523, 85 pp

Moran MD, Pielke RA (1996a) Evaluation of a mesoscale atmospheric dispersion modeling system with observations from the 1980 Great Plains mesoscale tracer field experiment. Part I: Data sets and meteorological simulations. J Appl Meteor 35: 281–307

Moran MD, Pielke RA (1996b) Evaluation of a mesoscale atmospheric dispersion modeling system with observations from the 1980 Great Plains mesoscale tracer field experiment. Part II: Dispersion simulations. J Appl Meteor 35: 308–329

Mossop SC (1978) The influence of drop size distribution on the production of secondary ice particles during graupel growth. Q J Roy Meteor Soc 104: 323–330

Mukabana JR, Pielke RA (1996) Investigating the influence of synoptic-scale monsoonal winds and mesoscale circulations on diurnal weather patterns over Kenya using a mesoscale numerical model. Mon Wea Rev 124: 224–243

Nachamkin J, Cotton WR (2000) Interaction between a developing mesoscale convective system and its environment. Part II: Numerical simulation. Mon Wea Rev 128: 1225–1244

Nair US, Hjelmfelt MR, Pielke RA (1997) Numerical simulation of the June 9–10, 1972 Black Hills storm using CSU RAMS. Mon Wea Rev 125: 1753–1766

Nicholls ME, Pielke RA, Eastman JL, Finley CA, Lyons WA, Tremback CJ, Walko RL, Cotton WR (1995) Applications of the RAMS numerical model to dispersion over urban areas. In: Wind Climate in Cities (Cermak JE et al, eds). The Netherlands: Kluwer Academic Publishers, pp 703–732

Nicholls ME, Pielke RA, Cotton WR (1991a) A two-dimensional numerical investigation of the interaction between sea-breezes and deep convection over the Florida peninsula. Mon Wea Rev 119: 298–323

Nicholls ME, Pielke RA, Cotton WR (1991b) Thermally forced gravity waves in an atmosphere at rest. J Atmos Sci 48: 1869–1884

Nicholls ME, Pielke RA, Cotton WR (1993a) Reply to comments on "Thermally forced gravity waves in an atmosphere at rest." J Atmos Sci 50: 4102

Nicholls ME, Pielke RA, Eastman JL, Finley CA, Lyons WA, Tremback CJ, Walko RL, Cotton WR (1993b) Applications of the RAMS numerical model to dispersion over urban areas. In: The effect of urbanization on windfields, air pollution spreading, and wind forces (Plate EJ, ed). The Netherlands: Kluwer Academic Publishers, pp 703–732

Nicholls ME, Pielke RA, Meroney RN (1993c) Large eddy simulation of microburst winds flowing around a building. J Wind Eng Ind Aerod 46–47: 229–237

Nicholls ME, Pielke RA, Greco S, Emmitt D (2000) An investigation of the impact of including CAMEX-3 data on high resolution hurricane Bonnie simulations. 24th Conf. on Hurricanes and Tropical Meteorology, Fort Lauderdale, Florida

Olsson PQ, Harrington JY (2000) Dynamics and energetics of the cloudy boundary layer in simulations of off-ice flow in the marginal ice zone. J Geophys Res 105: 11889–11899

Pan D-M, Randall DA (1998) A cumulus parameterization with a prognostic closure. Q J Roy Meteor Soc 124: 949–981

Papineau J, Pielke RA, Wesley DA (1994) A performance evaluation of the NGM and RAMS models for the 29–30 March, 1991 Colorado Front Range Storm. Nat Wea Digest 19: 2–11

Peterka JA, Cermak JE (1976) Adverse wind loading induced by adjacent buildings. J Structural Division, Proc. of the Americal Society of Civil Engineers, 102, No. ST3, pp 533–548

Peterka JA, Cochran LS, Pielke RA, Nicholls ME (1996) Progress in modeling external atmospheric flows around buildings. FED-Vol. 238, 1996 Fluids Engineering Division Conf., Vol. 3, ASME

Petersen WA, Carey LD, Rutledge SA, Knievel JC, Doesken NJ, Johnson RH, McKee TB, Vonder Haar T, Weaver JF (1999) Mesoscale and radar observations of the Fort Collins flash flood of 28 July, 1997. Bull Amer Meteor Soc 80: 191–216

Pielke RA (1998) Climate prediction as an initial value problem. Bull Amer Meteor Soc 79: 2743–2746

Pielke RA (2001a) Earth system modeling – An integrated assessment tool for environmental studies. 14th Toyota Conf., Shizouka, Japan (submitted)

Pielke RA (2001b) Mesoscale meteorological modeling. New York: Academic Press (forthcoming)

Pielke RA (2001c) Influence of the spatial distribution of vegetation and soils on the prediction of cumulus convective rainfall. Rev Geophys (forthcoming)

Pielke RA Sr, Nicholls ME (1997) Use of meteorological models in computational wind engineering. J Wind Eng Ind Aerod 67–68: 363–372

Pielke RA, Uliasz M (1993) Influence of landscape variability on atmospheric dispersion. J Air Waste Mgt 43: 989–994

Pielke RA, Uliasz M (1998) Use of meteorological models as input to regional and mesoscale air quality models – Limitations and strengths. Atmos Environ 32: 1455–1466

Pielke RA, Dalu G, Snook JS, Lee TJ, Kittel TGF (1991a) Nonlinear influence of mesoscale land use on weather and climate. J Clim 4: 1053–1069

Pielke RA, Song A, Michaels PJ, Lyons WA, Arritt RW (1991b) The predictability of sea-breeze generated thunderstorms. Atmosfera 4: 65–78

Pielke RA, Cotton WR, Walko RL, Tremback CJ, Lyons WA, Grasso LD, Nicholls ME, Moran MD, Wesley DA, Lee TJ, Copeland JH (1992a) A comprehensive meteorological modeling system – RAMS. Meteorol Atmos Phys 49: 69–91

Pielke RA, Walko RL, Eastman JL, Lyons WA, Stocker RA, Uliasz M, Tremback CJ (1992b) Recent achievements in the meteorological modeling of local weather and air quality. Trends in Atmospheric Science 1: 287–307

Pielke RA, Lee TJ, Glenn EP, Avissar R (1993) Influence of halophyte plantings in arid regions on local atmosphere structure. Int J Biometeorol 37: 96–100

Pielke RA, Lee TJ, Copeland JH, Eastman JL, Ziegler CL, Finley CA (1997) Use of USGS-provided data to improve weather and climate simulations. Ecol Appl 7: 3–21

Pielke RA Sr, Dalu G, Eastman J, Vidale PL, Zeng X (1998) Boundary layer processes and land surface interactions on the mesoscale. In: Clear and Cloudy Boundary Layers (Holtslag AAM, Duynkerke PG, eds), chap. 7. Amsterdam: Royal Netherlands Academy of Arts and Sciences, pp 155–176

Pielke RA Sr, Liston GE, Lu L, Avissar R (1999a) Land-surface influences on atmospheric dynamics and precipitation. In: Integrating Hydrology, Ecosystem Dynamics, and Biogeochemistry in Complex Landscapes (Tenhunen JD, Kabat P, eds), chap. 6. New York: Wiley, pp 105–116

Pielke RA, Walko RL, Steyaert L, Vidale PL, Liston GE, Lyons WA (1999b) The influence of anthropogenic landscape changes on weather in south Florida. Mon Wea Rev 127: 1663–1673

Pielke RA, Liston GE, Eastman JL, Lu L, Coughenour M (1999c) Seasonal weather prediction as an initial value problem. J Geophys Res 104: 19463–19479

Poulos GS, Pielke RA (1994) A numerical analysis of Los Angeles basin pollution transport to the Grand Canyon under stably stratified, southwest flow conditions. Atmos Environ 28: 3329–3357

Proctor FH (1989) Numerical simulations of an isolated microburst. Part 2: Sensitivity experiments. J Atmos Sci 46: 2143–2165

Rafkin SCR (1996) Development of a cumulus parameterization suitable for use in mesoscale through GCM-Scale models. PhD Diss., Atmospheric Science Paper #611, Colorado State University, Department of Atmospheric Science, Fort Collins, CO 80523, 126 pp

Rangno AL, Hobbs PV (1991) Ice particle concentrations and precipitation development in small polar maritime cumuliform clouds. Q J Roy Meteor Soc 117: 207–241

Rangno AL, Hobbs PV (1994) Ice particle concentrations and precipitation development in small continental cumuliform clouds. Q J Roy Meteor Soc 120: 573–601

Reisin T, Levin Z, Tzivion S (1996) Rain production in convective clouds as simulated in an axisymmetric model with detailed microphysics. Part I: Description of model. J Atmos Sci 53: 497–519

Schmidt JM (1985) Structure and evolution of a squall line with an embedded supercell. MS Thesis, Colorado State University, Department of Atmospheric Science, Fort Collins, CO 80523, 141 pp

Shook K, Gray DM, Pomeroy JW (1993) Temporal variation in snowcover area during melt in prairie and alpine environments. Nord Hydrol 24: 183–198

Shaw BL, Pielke RA, Ziegler CL (1997) A 3D numerical simulation of a Great Plains dryline. Mon Wea Rev 125: 1489–1506

Smagorinsky J (1963) General circulation experiments with the primitive equations. Part I: The basic experiment. Mon Wea Rev 91: 99–164

Snook JS, Pielke RA (1995) Diagnosing a Colorado heavy snow event with a nonhydrostatic mesoscale numerical

model structured for operational use. Wea Forecast 10: 261–285

Starr DO'C (1987) Cirrus-cloud experiment: Intensive field observations planned for FIRE. Bull Amer Met Soc 68: 119–124

Stevens B, Cotton WR, Feingold G (1998) A critique of one- and two-dimensional models of boundary layer clouds with a binned representation of drop microphysics. J Atmos Res 47–48: 529–533

Stohlgren JT, Chase TN, Pielke RA, Kittel TGF, Baron J (1998) Evidence that local land use practices influence regional climate and vegetation patterns in adjacent natural areas. Glob Change Biol 4: 495–504

Sturm M, Holmgren J, Liston GE (1995) A seasonal snow cover classification system for local to global applications. J Clim 8: 1261–1283

Takle ES, Gutowski WJ Jr, Arritt RW, Pan A, Anderson CJ, de Silva RR, Caya D, Chen S-C, Giorgi F, Christensen JH, Hong S-Y, Juang HM-H, Katzfey J, Lapenta WM, Laprise R, Liston GE, Lopez P, McGregor J, Pielke RA Sr, Roads JO (1999) Project to Intercompare Regional Climate Simulations (PIRCS) description and initial results. J Geophys Res 104: 19443–19461

Taylor CM, Harding RJ, Pielke RA Sr, Vidale PL, Walko RL, Pomeroy JW (1998) Snow breezes in the boreal forest. J Geophys Res 103: 23087–23101

Tremback CJ (1990) Numerical simulation of a mesoscale convective complex: Model development and numerical results. PhD Diss., Atmos Sci Paper No 465, Colorado State University, Department of Atmospheric Science, Fort Collins, CO 80523

Tremback CJ, Kessler R (1985) A surface temperature and moisture parameterization for use in mesoscale models. Proc. 7th Conf. on Numerical Weather Prediction, Boston, MA, AMS, pp 355–358

Tripoli GJ, Cotton WR (1982) The Colorado State University three-dimensional cloud/mesoscale model – 1982. Part I: General theoretical framework and sensitivity experiments. J Rech Atmos 16: 185–220

Tripoli GJ, Cotton WR (1986) An intense, quasi-steady thunderstorm over mountainous terrain. Part IV: Three-dimensional numerical simulation. J Atmos Sci 43: 896–914

Tripoli GJ, Cotton WR (1989a) A numerical study of an observed orogenic mesoscale convective system. Part 1: Simulated genesis and comparison with observations. Mon Wea Rev 117: 273–304

Tripoli GJ, Cotton WR (1989b) A numerical study of an observed orogenic mesoscale convective system. Part 2: Analysis of governing dynamics. Mon Wea Rev 117: 305–328

Tzivion S, Feingold G, Levin Z (1987) An efficient numerical solution to the stochastic collection equation. J Atmos Sci 44: 3139–3149

Uliasz M, Stocker RA, Pielke RA (1996) Regional modeling of air pollution transport in the southwestern United States. In: Environmental Modeling, Vol. III (Zannetti P, ed), chap. 5. Computational Mechanics Publications, pp 145–181

Vali G (1974) Contact ice nucleation by natural and artificial aerosols. Conf. on Cloud Physics, Tucson, AZ, Amer Meteor Soc, pp 34–37

Vali G (1976) Contact-freezing nucleation measured by the DFC instrument. 3rd Int. Workshop on Ice Nucleus Measurements. Laramie, Univ. of Wyoming, pp 159–178

Verlinde J, Flatau PJ, Cotton WR (1990) Analytical solutions to the collection growth equation: Comparison with approximate methods and application to cloud microphysics parameterization schemes. J Atmos Sci 47: 2871–2880

Vidale PL, Pielke RA, Barr A, Steyaert LT (1997) Case study modeling of turbulent and mesoscale fluxes over the BOREAS region. J Geophys Res 102: 29167–29188

Walko RL, Tremback CJ, Pielke RA, Cotton WR (1995) An interactive nesting algorithm for stretched grids and variable nesting ratios. J Appl Meteor 34: 994–999

Walko RL, Band LE, Baron J, Kittel TGF, Lammers R, Lee TJ, Ojima D, Pielke RA Sr, Taylor C, Tague C, Tremback CJ, Vidale PJ (2000) Coupled atmosphere-biophysics-hydrology models for environmental modeling. J Appl Meteor 39: 931–944

Walko RL, Cotton WR, Pielke RA (1992) Large-eddy simulations of the effects of hilly terrain on the convective boundary layer. Bound-Layer Meteor 58: 133–150

Weissbluth MJ (1991) Convective parameterization in mesoscale models. PhD Diss., Atmos Sci Paper No 486, Colorado State University, Department of Atmospheric Science, Fort Collins, CO 80523, 211 pp

Wu T (1999) Numerical modeling study of the November 26, 1991 cirrus event. PhD Diss., Colorado State University, Department of Atmospheric Science, Fort Collins, CO 80523, 188 pp

Wu T, Cotton WR, Cheng WYY (2000) Radiative effects on the diffusional growth of ice particles in cirrus clouds. J Atmos Sci 57: 2892–2904

Young KC (1974a) A numerical simulation of wintertime, orographic precipitation: Part I: Description of model microphysics and numerical techniques. J Atmos Sci 31: 1735–1748

Young KC (1947b) A numerical simulation of wintertime, orographic precipitation: Part II: Comparison of natural and agI-seeded conditions. J Atmos Sci 31: 1749–1767

Xian Z, Pielke RA (1991) The effects of width of land masses on the development of sea breezes. J Appl Meteor 30: 1280–1304

Ziegler CL, Martin WJ, Pielke RA, Walko RL (1995) A modeling study of the dryline. J Atmos Sci 52: 263–285

Ziegler CL, Lee TJ, Pielke RA (1997) Convective initiation at the dryline: A modeling study. Mon Wea Rev 125: 1001–1026

Corresponding author's address: Dr. William R. Cotton, Department of Atmospheric Science, Colorado State University, Fort Collins, CO 80523-1371, U.S.A. (E-mail: cotton@atmos.colostate.edu)